

**YILDIRIM BEYAZIT UNIVERSITY**  
**GRADUATE SCHOOL OF NATURAL AND APPLIED SCIENCES**



**A STUDY ON THE MECHANICS OF AN ELECTRICALLY  
ACTUATED MICRO CANTILEVER BEAM SWITCH**

**M.Sc. Thesis by**

**M. Cihat YILMAZ**

**Department of Mechanical Engineering**

**August, 2016**

**ANKARA**

**A STUDY ON THE MECHANICS OF AN ELECTRICALLY  
ACTUATED MICRO CANTILEVER BEAM SWITCH**

**A Thesis Submitted to the  
Graduate School of Natural and Applied Sciences of Yıldırım Beyazıt University  
In Partial Fulfillment of the Requirements for the Master of Science in  
Electronics and Communication Engineering, Department of Electronics and  
Communication Engineering**

**by**

**M. Cihat YILMAZ**

**August, 2016**

**ANKARA**

## M.Sc. THESIS EXAMINATION RESULT FORM

We have read the thesis entitled “**A Study on the Mechanics of an Electrically Actuated Micro Cantilever Beam Switch**” completed by **Mahmut Cihat YILMAZ** under supervision of **Prof. Dr. Sadettin ORHAN** and we certify that in our opinion it is fully adequate, in scope and in quality, as a thesis for the degree of Master of Science.

.....  
Prof. Dr. Sadettin ORHAN

\_\_\_\_\_  
**(Supervisor)**

.....  
Prof. Dr. Mehmet Ali GÜLER

\_\_\_\_\_  
**(Jury Member)**

.....  
Assoc. Prof. Dr. Arif ANKARALI

\_\_\_\_\_  
**(Jury Member)**

.....  
Prof. Dr. Fatih V. ÇELEBİ

\_\_\_\_\_  
**(Director)**

Graduate School of Natural and Applied Sciences

## **ETHICAL DECLARATION**

I have prepared this dissertation study in accordance with the Rules of Writing Thesis of Yıldırım Beyazıt University of Science and Technology Institute;

- Data I have presented in the thesis, information and documents that I obtained in the framework of academic and ethical rules,
- All information, documentation, assessment and results that I presented in accordance with scientific ethics and morals,
- I have gave references all the works that I were benefited in this dissertation by appropriate reference,
- I would not make any changes in the data that I were used,
- The work presented in this dissertation I would agree that the original,

I state, in the contrary case I declare that I accept the all rights losses that may arise against me.

## **ACKNOWLEDGEMENTS**

I owe my mother, my father, my brother, my grandparents and my wife a debt of gratitude for their endless encouragement and blessing before and during the period of my M.Sc. I would like to thank to my colleagues especially Metin ÖZTÜRK for their help whenever I need.

I also want to thank to Dr. Mehmet ÜNLÜ for bringing me in to this great subject and everything he taught me, Assoc. Prof. Arif ANKARALI, Prof. Dr. Alaattin AKTAŞ and Prof. Dr. Osman YİĞİT for their precious supports.

Finally, special gratitude to my advisor Prof. Dr. Sadettin ORHAN for his efforts, patience and making me feel this department like home until the first day.

**2016, 10 August**

**M. Cihat YILMAZ**

# **A STUDY ON THE MECHANICS OF AN ELECTRICALLY ACTUATED MICRO CANTILEVER BEAM SWITCH**

## **ABSTRACT**

RF MEMS, which is becoming RF NEMS (Radio Frequency Nano Electro Mechanical Systems) nowadays via emergent science, are very important for communication technology. Therefore, minimizing the sizes is essential to achieve higher frequency, faster switching, lower actuation voltage and to enlarge application areas. In this thesis study, RF MEMS switches are briefly introduced. A relatively smaller metal to metal contact, series RF MEMS switch is designed and its mechanical parameters are investigated. A hole is used in design to reduce the stiffness. The distributed load that occurs on the designed beam due to the applied voltage is calculated. Deflection of the beam is determined using principles of mechanics. Hence, three types of stiffness are calculated. This calculation method is verified with a similar design that is taken from literature. Resonant frequency, pull-in voltage, hold-down voltage, switching time, release time, contact force and release force are studied and simulated. For release force calculation, two different approaches are discussed. Solution results and simulation results are compared with each other and the failure ratios are discussed. In addition to this, residual stress effect on the deflection is mentioned. Also a new approach is brought for pull\_in voltage calculation and its flow-chart is given. For simulation MATLAB and Coventor software are used.

**Keywords:** RF MEMS, switches, cantilever beam, stiffness, pull\_in voltage, contact force

# ELEKTRİKSEL OLARAK HAREKET ETTİRİLEN ANKASTRE MESNETLİ BİR MİKRO KİRİŞİN MEKANİĞİ ÜZERİNE BİR ÇALIŞMA

## ÖZET

Son zamanlarda gelişen teknoloji ile artık RF NEMS (Radyo Frekansı Nano Elektro Mekanik Sistemler) olarak da anılmaya başlanan RF MEMS, iletişim teknolojisi için çok önemli bir yere sahiptir. Bu yüzden boyutların küçülmesi, yüksek frekansa ulaşmak, hızlı anahtarlama sağlamak, düşük voltaj harcamak ve uygulama alanlarını genişletmek açısından oldukça önemlidir. Bu tez çalışmasında RF MEMS anahtarları kısaca tanıtılmış, görece küçük, metal temaslı, sinyali kendi üzerinden ileten bir RF MEMS anahtar yapısı tasarlanarak bunun mekanik parametreleri incelenmiştir. Tasarımda bir delik kullanılarak rijitliğin azaltılması hedeflenmiştir. Tasarlanan ankastre mesnetli kiriş yapısının üzerinde voltaj uygulanmasıyla oluşan yayılı yük hesaplanmıştır. Bu yayılı yükün yapacağı sehim temel mukavemet prensipleriyle elde edilmiş ve buradan hareketle üç çeşit yay sabiti hesaplanmıştır. Bu çözüm yöntemi literatürden alınan ve tasarımı benzer bir kiriş modeli üzerinde de doğrulanmıştır. Rezonans frekansı, çökme voltajı, basılı tutma voltajı, çökme süresi, serbest kalma süresi, temas kuvveti ve salıverme kuvveti gibi parametreler çalışılmış ve simülasyonu yapılmıştır. Salıverme kuvveti için iki farklı yaklaşım tartışılmıştır. Çözüm sonuçları ile simülasyon sonuçları birbiriyle kıyaslanarak hata oranları tartışılmıştır. Buna ilave olarak, kalıntı stresinin sehim üzerindeki etkisinden de bahsedilmiştir. Ayrıca çökme voltajı hesabı için yeni bir yaklaşım getirilmiş ve bunun akış şeması gösterilmiştir. Simülasyon ve hesaplamalarda MATLAB ve COVENTOR programları kullanılmıştır.

**Anahtar Kelimeler:** RF MEMS, anahtarlar, ankastre mesnetli kiriş, rijitlik, çökme voltajı, temas kuvveti

# CONTENTS

	Page
<b>M.Sc. THESIS EXAMINATION RESULT FORM .....</b>	<b>ii</b>
<b>ETHICAL DECLARATION .....</b>	<b>iii</b>
<b>ABSTRACT .....</b>	<b>iv</b>
<b>ÖZET .....</b>	<b>v</b>
<b>ACKNOWLEDGEMENTS.....</b>	<b>vi</b>
<b>CONTENTS.....</b>	<b>vii</b>
<b>LIST OF TABLES .....</b>	<b>ix</b>
<b>LIST OF FIGURES .....</b>	<b>x</b>
<b>CHAPTER 1 - INTRODUCTION.....</b>	<b>1</b>
1.1 RF MEMS History .....	1
<b>CHAPTER 2 - RF MEMS SWITCHES.....</b>	<b>9</b>
2.1 What is RF MEMS .....	9
2.2 RF MEMS Switches .....	12
2.3 RF MEMS Switch Types .....	14
2.4 Fabrication and Packaging of RF MEMS .....	16
<b>CHAPTER 3 - MECHANICAL PARAMETERS OF A CANTILEVER BEAM TYPE RF MEMS SWITCH.....</b>	<b>20</b>
3.1 Stiffness of Cantilever Beam.....	20
3.1.1 Deflection Under Electrical Actuation .....	20



3.1.2 Natural Spring Constant .....	34
3.1.3 Actuation Spring Constant .....	36
3.1.4 Release Spring Constant.....	40
3.2 Calculations of Other Switch Parameters.....	42
3.2.1 Pull_In Voltage.....	43
3.2.2 Contact Force .....	47
3.2.3 Release Force .....	55
3.2.4 Resonant Frequency and Switch Time.....	60
3.2.5 Air Damping And Release Time.....	63
3.2.6 Stress Effect.....	66
3.3 Simulation Results of Designed Switch.....	68
<b>CHAPTER 4 – CONCLUSIONS.....</b>	<b>78</b>
<b>REFERENCE .....</b>	<b>80</b>
<b>APPENDIX A .....</b>	<b>88</b>
<b>RESUME.....</b>	<b>89</b>

**LIST OF TABLES**

**Table 3.1** The geometry variables in  $\mu m$  unit for cantilever beam model.....30  
**Table 3.2** Comparison of switch characteristics results for beam model ..... 75  
**Table 3.3** Simulation for different geometric parameters ..... 76



## LIST OF FIGURES

<b>Figure 1.1</b> Tethered cantilever beam RF MEMS switch [7].....	3
<b>Figure 1.2</b> Examples of small switches from literature [20-25-23-21].....	7
<b>Figure 2.1</b> Electromagnetic spectrum [38].....	9
<b>Figure 2.2</b> Frequency range [39].....	10
<b>Figure 2.3</b> RF MEMS technology roadmap [41].....	10
<b>Figure 2.4</b> A cell puller which measures the mechanical properties of a living cell [48].....	11
<b>Figure 2.5</b> Cantilever beam type RF MEMS switch.....	13
<b>Figure 2.6</b> Cantilever (left) and fixed-fixed beam switches.....	14
<b>Figure 2.7</b> Switch types: (a) shunt metal-contact switch (b) shunt capacitive switch (c) series metal-contact switch (d) series capacitive switch.....	15
<b>Figure 2.8</b> Building steps of simulation program.....	16
<b>Figure 2.9</b> Mask layers that used in fabrication.....	17
Figure 2.10 Schematic view of RF MEMS switch fabrication steps.....	18
<b>Figure 2.11</b> (a) and (b) real pictures of packaged switches (c) on-wafer hermetic packaging of mems switches [55-56].....	19
<b>Figure 3.1</b> Three times exaggerated isometric view and side view of a bended cantilever beam under actuated voltage.....	20
<b>Figure 3.2</b> Side view of an actuated beam.....	22
<b>Figure 3.3</b> The distributed load is simplified as linear.....	23
<b>Figure 3.4</b> (a) Separated distributed load, (b) The top view of distributed load and the cutting line.....	24
<b>Figure 3.5</b> The concentrated loads and the superposition method.....	25
<b>Figure 3.6</b> Cutting of AB part from an $x$ point.....	27
<b>Figure 3.7</b> Additional deflection at the center due to the hole.....	29
<b>Figure 3.8</b> Dimensions from top view of the beam.....	31
<b>Figure 3.9</b> Calculation for $q$ and $q'$ .....	32
<b>Figure 3.10</b> Superposition for natural stiffness.....	34
<b>Figure 3.11</b> Finding of the center of gravity of the distributed load.....	37
<b>Figure 3.12</b> Concentrated load at the center of gravity.....	38
<b>Figure 3.13</b> Concentrated load is at the end for release stiffness.....	42

<b>Figure 3.14</b> Flowchart of pull_in voltage calculation .....	45
<b>Figure 3.15</b> Shape of the beam at contact situation.....	48
<b>Figure 3.16</b> Moment diagrams of distributed load at contact situation.....	51
<b>Figure 3.17</b> Moment diagrams of distributed load and unit load at contact situation.....	52
<b>Figure 3.18</b> Mechanical and electrical contact surfaces [64] .....	55
<b>Figure 3.19</b> Simulation image for contact situation .....	56
<b>Figure 3.20</b> Realistic release force .....	56
<b>Figure 3.21</b> Second restoring force approach.....	59
<b>Figure 3.22</b> Stress gradient at the end of the beam .....	66
<b>Figure 3.23 (a)</b> Side view of cantilever beam design <b>(b)</b> Meshed and 3 times extended view .....	68
<b>Figure 3.24</b> Resonant frequencies of the beam .....	69
<b>Figure 3.25</b> Summary of pull_in simulation .....	69
<b>Figure 3.26</b> Summary of sensitive pull_in simulation .....	70
<b>Figure 3.27</b> Position of figure against gap .....	71
<b>Figure 3.28</b> Total electrostatic force on the beam at collapse instant .....	71
<b>Figure 3.29</b> Summary of sensitive hold-down voltage simulation.....	72
<b>Figure 3.30</b> Contact force simulation.....	73
<b>Figure 3.31</b> Reaction forces of fixed end of the beam .....	73
<b>Figure 3.32</b> Time analysis in Coventor .....	74

# CHAPTER 1

## INTRODUCTION

Nanotechnology is a very fashionable horizon line for almost all branches of science. Down-sizing the vehicles, structures, machines and devices etc. is sometimes necessity for current applications and sometimes a plunge point for future works. As well, RF MEMS (Radio Frequency Micro Electro Mechanical Systems) technology that is used in wireless communication, defense systems, test and instrumentation areas, was born as a result of this minimalize movement.

For RF MEMS technology, it would be fitting to say that, there are two main innovations that effects the communication technology; switching and phase shifting.

### 1.1 RF MEMS History

Switching is a vital factor for most of the electronic applications such as communication systems, power electronics and so on. A switch is an electronic device that can stop and allow the current flow in electrical networks.

It is necessary to look a little back in history in order to understand the RF MEMS switches. FETs (Field Effect Transistors) have been used as microwave switch for a long time as mentioned by H. A. Atwater and R. W. Sudbury in 1981. Mainly, a systematical standard for the description of microwave and millimeter wave modulations is studied. They worked about the parameters that affects the switching quality factor which was determined by Kurokawa and Schlosser. It is also mentioned that FET's are proper for monolithic integration. Hine's power theorem is used to determine the switching power limitations. Atwater and Sudbury also reveals that the power handling capacity of FET switches is simply depended on the breakdown and pinch off voltages [1].

In 1985, a study shows that GaAs (Gallium Arsenide) FET devices are used for two state RF switch as phase shifter or TR switch. The authors' switch design enhanced the switching quality factor while the power handling capacity is not changed. Switch parameters are obtained by analytical method and two-dimensional simulation. The quality factor is found depended on impedance states of the switch. In theory calculations, basic parallel plate capacitance theory is used and finally the obtained idea is that, decreasing the gate-source, gate-drain and gate dimensions increases the quality factor and thereby the switch performance [2].

The RF MEMS switch, which was designed by Dr. Larry Larson in 1990, is considered as the first one [3]. The main purpose of this study was improving the conventional MMIC technique by applying micro-machined microwave actuator (MIMAC) technology to GaAs MMICs. Fabrication process and optimized microwave actuator structure were considered, and it was understood that MIMAC processing is compatible with GaAs MMIC processing. After experimental studies, insertion loss of around 0.4 *dB* and higher than 35 *dB* isolation have achieved for the frequency range between 2 and 45 *GHz*. Results belonging to MIMAC technology are similar to conventional switching applications while volume has decreased [4].

In a study about membrane switches is presented by C. Goldsmith and T. H. Lin. The authors mentioned that, micro sized cantilever beam structures were used for low frequency electrical signal switching for the first time in 1979. The handicaps of these early works are being not able to create suitable contact force and requiring much more actuation voltage. Even so, revision of dimensions and materials have been opened a road for microwave switches. Unambiguously, they studied low-loss, low-cost, electrically actuated, thin metal membrane switches and build some variety of them. They frequently compared their results with GaAs and CMOS technology. One of the sizes of their switches are 700 x 800  $\mu m$ , pull-in voltage of nearly 40 *V*. In addition, they revealed that the switching time is about 10 to a couple hundred micro seconds [5].

A study of G. M. Rebeiz shows the most current development about micro-machined switches at the beginning of new millennium. Also performances of several fabricated and published switches are compared with each other. It is mentioned that to use RF MEMS switches more logical than pin diodes or FET switches due to higher performance and other reasons like very high isolation, low insertion loss and intermodulation products. As the disadvantages, reliability, packaging, cost and power handling are the given examples. Fabrication and performance of series switches and also packaging techniques are mentioned. Rebeiz describes the little switch that could as that Lincoln Labs developed which is in  $8 \times 45 \mu\text{m}$  sizes at the time this paper written [6].

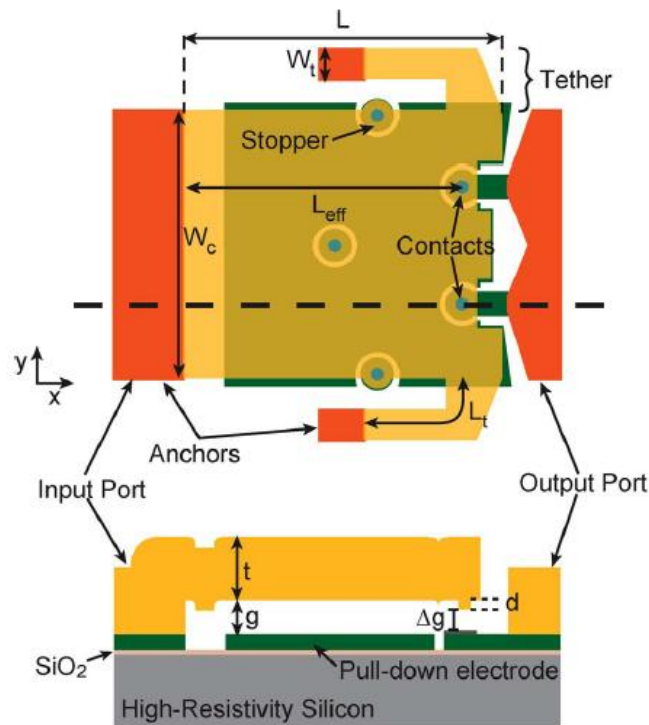


**Figure 1.1** Tethered cantilever beam RF MEMS switch [7]

Another study of Rebeiz with C. D. Patel demonstrates the up to date of RF MEMS switch technology. In this study the authors developed a new switch design to increase stiffness and reduce residual stress effects. Tethers that used at the free end of the cantilever beam

switch for this aim are shown at Figure 1.1. Mathematical model of the beam with tethers are presented and stiffness is found as three parallel springs model. They demonstrated simplified formulas for spring constant and contact force calculations. Contact force depends on the length and the stiffness of the beam and the gap between the bridge and the underlying electrode which is used for electrostatic movement. The beam structure is made of an  $8 \mu\text{m}$  Ti/Au layer. The sizes and the pull-down voltage of the beam are  $155 \times 130 \mu\text{m}$  and about  $60 \text{ V}$  respectively while the switching time is  $5 - 6 \text{ us}$ . Effects of stress gradients and biaxial stress are also studied which exhibits that the stress gradient induces a great effect on variables like contact force and pull-in voltage [7].

In designing an RF MEMS switch, it is needed to choose a switch type according to the operation as mentioned by S. Suganthi and K. Murugesan in their study. In this paper, the effect of isolation and resonance frequency on the electrical performance of an RF MEMS switch which is used for satellite communication is discussed. To determine a switch type according to the application and frequency of operation is the first step of a system design. They used capacitive shunt RF MEMS switch due to containing less parasites and being able to handling more RF power. After choosing the switch type, different CPW (coplanar waveguide: a kind of electrical transmission line) configurations tested and they noticed that better performance came with CPW coupler which has two conductors connected among other CPW designs. Additionally, they trained artificial neural networks by comparison with simulation results [8].

A different metal contact switch model that leads to variable stiffness was designed by Pisheh and Rebeiz in 2010. The difference is placing a dimple before the free end of the cantilever and make the signal pass through it with a high contact force, when still the free end of the cantilever touches the dielectric layer. The contact force is obtained between  $0.6-1.1 \mu\text{N}$  for averagely  $80 \text{ V}$  applied voltage. After the voltage applied to the beam, first the free end touches the dielectric part and then the dimple touches the contact pad. Because of this two touching period, two stiffness level occurs and the dielectric layer



leads a decrease in contact resistance. Geometry of the gold switch is  $7 \times 150 \times 170 \mu m$  and  $SiN$  is used as dielectric layer [9].

S. C SAHA studied the spring constant and the pull-down voltage of a non-uniform  $100/125 \mu m$  lengthy cantilever beam type RF MEMS switch. He modeled the beam's width in two part; he put the actuation pad under the part that closer to free end and made this part wider than the part that closer to anchor. He also modeled the residual (tensile) stress which increases the gap but the calculations for it just done with Rebeiz's pull\_in voltage formula. This nonlinear switch is modeled both as capacitive switch and metal contact switch and also a comparison is made between analytical and simulation results [10].

Other most common RF MEMS components are phase shifters that provide to control to shift the phase of an RF signal. Older models are based on pin diodes and FET switches, and while they introduce lots of loss, RF MEMS phase shifters have some advantageous like easier hermetic packaging (even if not being straightforward), being cheaper and being able to fit more part in per wafer. The author indicates a handicap of RF MEMS phase shifters that because of being composed of nearly 10-15 switches, there is no chance to be a failure at any of them. Also, the performances of X-band and Ka-band MEMS phase shifters that produced by Raytheon, Rockwell Scientific and Michigan University are examined in this article. These works indicate about  $2.2 \text{ dB}$  insertion loss and associated bandwidth of nearly  $35 \text{ GHz}$  [11].

There are plenty of studies with design optimization have been done for mechanical concerns that include decreasing the actuation voltage, higher dynamic stiffness, smaller sizes, high switching speed, high contact force and also different actuation mechanisms like magnetically actuating are examined. Lots of parameters like different materials, gap values and geometry are experienced and also residual stress effect is taken into consideration in accordance with this aim. For material selection, a comparison shows that the lowest pull\_in voltage value comes with aluminum beam and gold, copper and nickel

follow it. Using holes on the beam structure leads to decrease spring constant, therefore actuation voltage. Also, it is demonstrated that the pull\_in voltage of fixed-fixed beam is higher than cantilever beam. Generally, it is hard to use the word 'ideal' for RF MEMS switches, for example, trying to decrease the actuation voltage results in bigger sizes on the other side so 'optimal' is more proper word for designing. An optimal design that is made lately, claimed a switching time about  $0.6 \mu s$  under an actuation voltage of  $14V$ . All these studies are being done with software programs like Coventor, COMSOL Multiphysics and ANSYS and results compared with analytical results and sometimes with neural networks method [12-18].

From a size point of view, RF MEMS switches are started to be developed at sizes of  $500 \mu m - 1 mm$  and nowadays, about  $1 \mu m$  sized switches can be seen in literature. A graphene type NEMS switch that sized  $7 \times 5 \mu m$  is produced by Rui Ma, Qi Chen in May 2016. Another very small switch designed by Anirudha V. Sumant in 2014. It is a fixed-fixed type  $0.1 \times 2 \mu m$  sized diamond film and yet it needs to improve in mechanical and electrical performance more. In 2015, Clara F. Moldovan built a capacitive fixed-fixed NEMS switch that consist of multilayer graphene membrane instead of monolayers that have lower resistance. This multilayer graphene is deposited by wet transfer using a transfer polymer. Four different examples of small sized switches that built lately by V. Sumant, P. Sharma, Z. Han and L. Boodhoo are shown in fig respectively [19-25].

The reliability of RF MEMS switches is a substantial issue that researchers care about and there are lots of publications about reliability and lifetime of RF MEMS. Reliability is a term of doing the given duty in a same accuracy in long term and generally related with physical hurt, planar hollows and toughness of the contact area between the beam structure and the transmission metal. Mechanical effects due to the friction between contact metals and thermal effects that lead to resistive heating again due to contact physic. These problems may result in to not to switch properly and the most helpful solution is packaging. Lifetimes of switches are measured with repetitive actuation voltages and it is

generally about  $10^5$ - $10^{10}$  cycles. Using dielectric layer is tested to overcome reliability problems in some of the studies. Some other authors studied the effect of temperature and indicate that  $55\text{ }^\circ\text{C}$  is good enough for better switching. Another paper shows the effect of fabrication tolerance on the performance of switching. These studies also say that other problems like contamination or organic residuals are avoidable with a fabrication in clean room conditions [26-31].

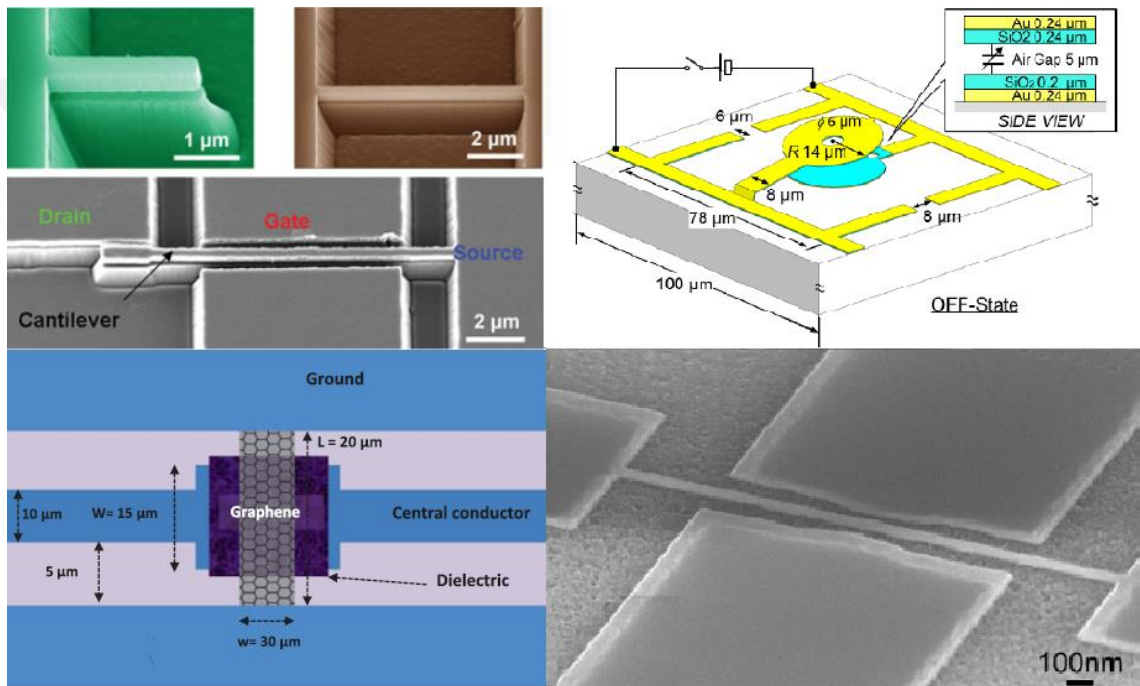


**Figure 1.2** Examples of small sized switches from literature [20-25-23-21]

Due to the reliability problems, it is still infrequent to use in industry in spite of a lot of study in the literature. There are several papers show the used RF MEMS devices commercially. Bulk acoustic wave filters may be considered as the first example of commercial RF MEMS devices and Magfusion Teravicta and Radant MEMS are shown as spearhead of commercialization. In another newer example, a tunable filter designed and fabricated using good linearity capacitors that manufactured by Cavendish Kinetics. Characteristic and lifetime evaluations of commercial switches are done according to their

usage area. Institutions and companies like Motorola, Agilent, Intel, IBM, NEC, LG, Samsung, Hughes Research Labs, U.S. Air Force Research Lab etc. that manufacture RF MEMS switches are indicated in this studies [32-36].

As demonstrated in literature examples above, it is very advantageous to use RF MEMS switches in communication systems due to the mentioned reasons. This study is mostly focused on the mechanics of an RF MEMS switch that has a cantilever beam type structure. The fundamental analysis is based on stiffness of the beam which effects the movement of the switch via an applied voltage. Besides, resonant frequency, switching time and contact force of the switch are also studied. All these calculations are sampled with a new design that has a smaller size from on-going studies. Lastly, a new approach is developed in order to obtain one of the desired variables and its verification is performed using MATLAB software platform.

This thesis is composed of four sections. After this introduction section, a general information about RF MEMS and switches, switch types and fabrication of RF MEMS switches are given in Section 2. In Section 3, an RF MEMS cantilevered beam switch model is shown and some characteristic of it like stiffness, pull\_in voltage and contact force are calculated, after that, simulation results and calculation results are compared with each other and the differences are discussed. In fourth and final section, a conclusion is done to sum up the subject and ideas about future works of this study are shared.

# CHAPTER 2

## RF MEMS SWITCHES

Shortly looking at RF MEMS (Radio Frequency Micro Electro Mechanical Systems) and communication technology is needed to understand RF MEMS switches better.

### 2.1 What is RF MEMS

From the beginning of the history, mankind recognized only the visible light from all frequencies in the nature which is called electromagnetic spectrum. The electromagnetic spectrum is the collective term for all known frequencies and their linked wavelengths of the known photons. Then, after the infrared radiation was discovered in 1800 by William Herschel [37], inventions about frequency bandwidth has come one by one until the discovery of gamma rays in the beginning of the 20<sup>th</sup> century. Electromagnetic waves have three basic physical properties: the frequency  $f$ , wavelength  $\lambda$ , and photon energy  $E$ .

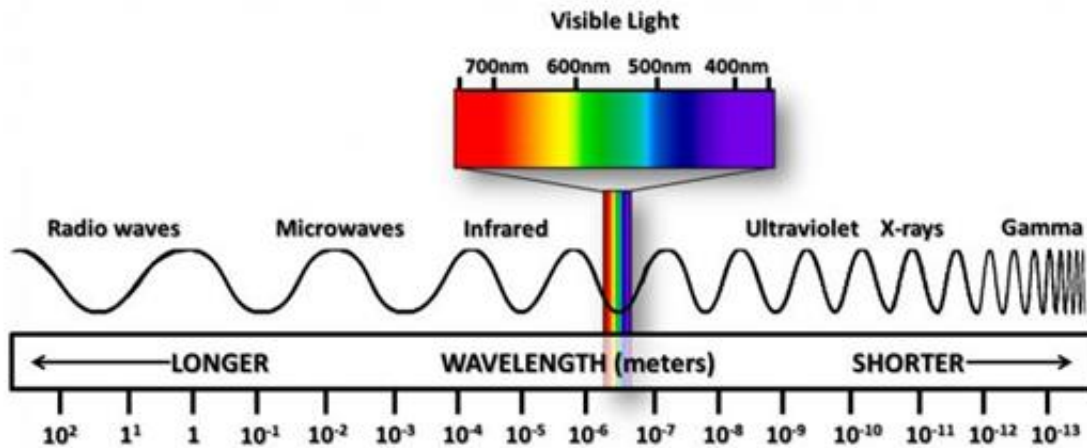
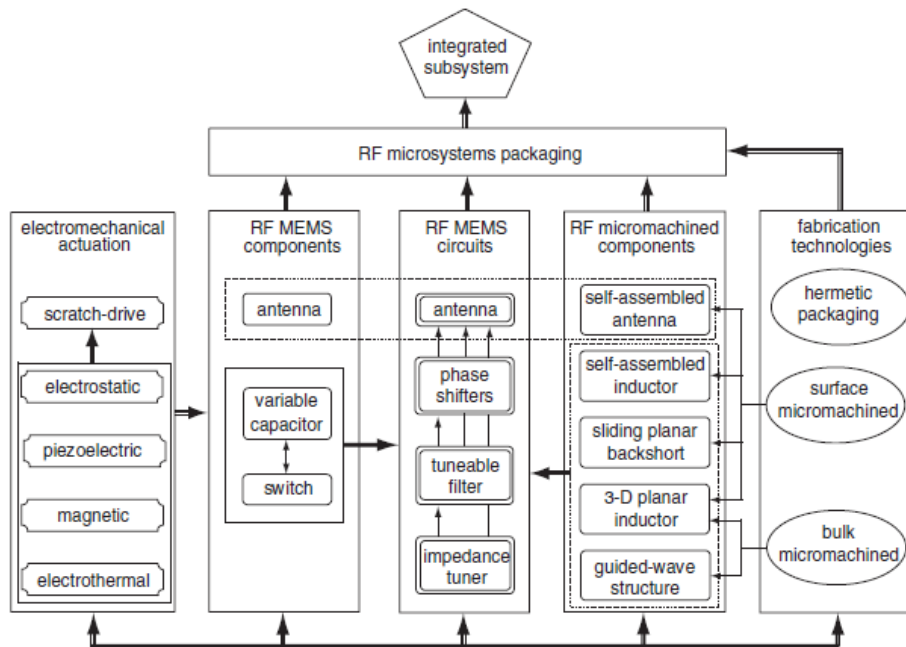


Figure 2.1 Electromagnetic spectrum [38]

f	$\lambda$	Band	Description
30-300 Hz	$10^4$ - $10^3$ km	ELF	Extremely low frequency
300-3000 Hz	$10^3$ - $10^2$ km	VF	Voice frequency
3-30 kHz	100-10 km	VLF	Very low frequency
30-300 kHz	10-1 km	LF	Low frequency
0.3-3 MHz	1-0.1 km	MF	Medium frequency
3-30 MHz	100-10 m	HF	High frequency
30-300 MHz	10-1 m	VHF	Very High frequency
300-3000 MHz	100-10 cm	UHF	Ultra-high frequency
3-30 GHz	10-1 cm	SHF	Super-high frequency
30-300 GHz	10-1 mm	EHF	Extremely high frequency (millimeter waves)

**Figure 2.2** Frequency ranges [39]

Among the electromagnetic spectrum, radio wave or radio frequency RF, that was discovered by Heinrich Hertz and has a bandwidth between 3 KHz and 300 GHz, have been using for communication [40].



**Figure 2.3** RF MEMS technology roadmap [41]

With the developing technology, the devices that generate, transmit and receive the RF signal became smaller. Thereby, this allowed the invention of mobile phones and satellite communication etc. Figure 2.3 expresses the general RF MEMS concept properly.

Briefly, RF MEMS are micro sized electronic devices that supply radio frequency performance and they are used in wireless, satellite and radar communication systems. But generally MEMS have a very wide range of application area like defense applications, automotive, navigation devices, earthquake detection and biotechnology [42].

Even if gradually decreasing, beside the usage of RF MEMS, compound semiconductor (GaAs, GaN etc.), ferrite, ferroelectric, CMOS (complementary metal oxide semiconductor) and vacuum tube technology are also being used for RF works [43-44]. Especially, GaAs PIN diodes and FETs (Field Effect Transistor) were mostly used switch types before RF MEMS switches for a long time but the advantageous of RF MEMS like consuming almost zero power, relatively very fast switching, being very small for high power application and other electronic features (capacitance ratio, isolation, loss, cutoff frequency) drive RF MEMS forward beyond others [45].

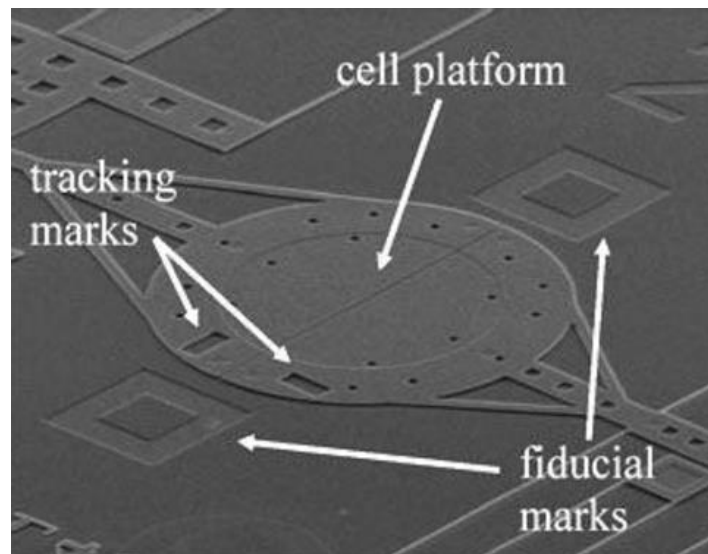


**Figure 2.4** A cell puller which measures the mechanical properties of a living cell [48]

The most common RF MEMS components are varactors, inductors and switches which are the subject of this thesis. Varactors are capacitors distinctly with adjustable voltage and inductors are circuit elements that generate electric current from potential difference [46-47].

Apart from all these, microelectromechanical systems are not only used in RF field but also used for accelerometers, gyroscopes, pressure sensors, microphones, and biomedical. Especially the existence of micro sensors leads most of profitable applications like cell phones, car tire pressure measurement and game controllers etc. in addition to these, bio MEMS illuminates the health industry with some innovations like blood pressure measurements and more. Figure 2.4 can be given as an example of it [49-53]. Still, this thesis is only focused on RF MEMS and in detail, RF MEMS switch.

## **2.2 RF MEMS Switches**

Although the fundamentals of MEMS technology bases on previous studies, first MEMS switches were studied as a laboratory study for low-frequency band. But, for microwave applications, Dr. Larry Larson designed the first RF MEMS switch [4].

RF MEMS switch can be basically defined as a micro sized electro-mechanical device that allows or not to an RF signal to pass through a signal transmission line. They are used to operate at radio frequency to millimeter wave frequency. They are assigned in electronic systems like signal filters, tunable antennas and phase shifters etc.

Their working principle is simple: to short or to open the electric circuit. For this purpose a controlled motion is needed. To make that motion, a capacitance which is controlled by an applied voltage is generated between two electrodes (structure and actuation pad). When a voltage applied to the beam via actuation pad lying under it, a distributed load occurs and forces the beam to bend. Although the distributed load is uniform at the very beginning of the motion, it starts to change after beam starts to bend and it goes on



sequentially so that an equilibrium occurs between the mechanical reaction force and total electrostatic force. When the voltage starts to be applied from zero and increased step by step, for all applied voltages before a specific voltage value, beam displaces and comes to an equilibrium position in which  $F_e$  due to applied voltage is equal to the mechanical reaction force  $F_r$ . If a voltage which is enough to make  $F_e$  bigger than  $F_r$ , applied to the beam, beam collapses. This specific voltage value is called pull\_in voltage. Figure 2.5 shows a schematic view of an RF MEMS switch.

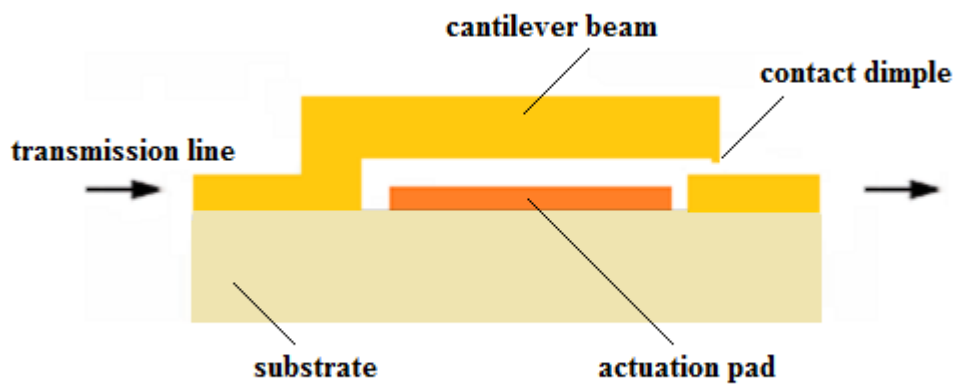


**Figure 2.5** Cantilever beam type RF MEMS switch

In parallel plate capacitance theory, beam collapses at  $g=(2/3)g_0$  where  $g$  is gap and  $g_0$  is the initial gap, because after this position, the reaction force cannot afford the total electrostatic force anymore. The parallel plate capacitance  $C$  is depended on the application area  $A$  and the gap between two metal  $g$ , as it is shown below [57].

$$C = \frac{\epsilon_0 A}{g} \tag{2.1}$$

where,  $\epsilon_0$  is permittivity constant [58]. After collapsing it is easier to keep the beam at down position than to get it down. It is called release or hold-down voltage and it is smaller than the pull\_in voltage inherently and around 10-20 V [6]. The duration that passes between the time that the voltage applied and the time that the beam settled down at down position is called switching time.

There are some side effects that make shorter the lifetime of the RF MEMS switches like creep and fatigue. Beam structures expose a load in a long term and a stress occurs on it, thus it deforms to relieve the stress, additionally, a residual stress may also occurs due to the manufacturing process which is not analyzed in this thesis. Contamination is another issue for RF MEMS devices because of having very small sizes, clean room conditions and packaging is needed that will be clarify in the next topic.

### 2.3 RF MEMS Switch Types

From mechanical perspective, RF MEMS switch structures are generally divided into two types: fixed-fixed beam and cantilever beam. Apart from these, special designs can be seen for RF MEMS switches like beams anchored from more than two place or radial disk design etc.

Fixed-fixed beam structures that used in RF MEMS applications called microbridges, the other most common beam type is in fixed-free form and generally called microcantilevers which is worked in this thesis.

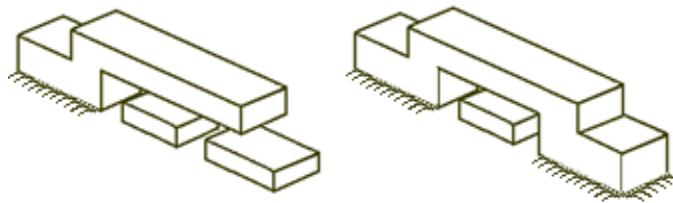


**Figure 2.6** Cantilever (left) and fixed-fixed beam switches

Beside from this constructive distinction, RF MEMS switches can be classified according to whether using of dielectric layer. On one hand, capacitive switches use dielectric layers on contact area and utilize electric field to transmit the signal, on the other hand, some switches don't use dielectrics and transmit the signal directly touching to the transmission line which is called metal to metal contact switch.

Another differentiation is made according to settling/layout; RF MEMS switches are designed as series or shunt. Basically, if the anchor/anchors of the beam is/are on the transmission line, it is series unless shunt, this can be understood better from the Figure 2.7.

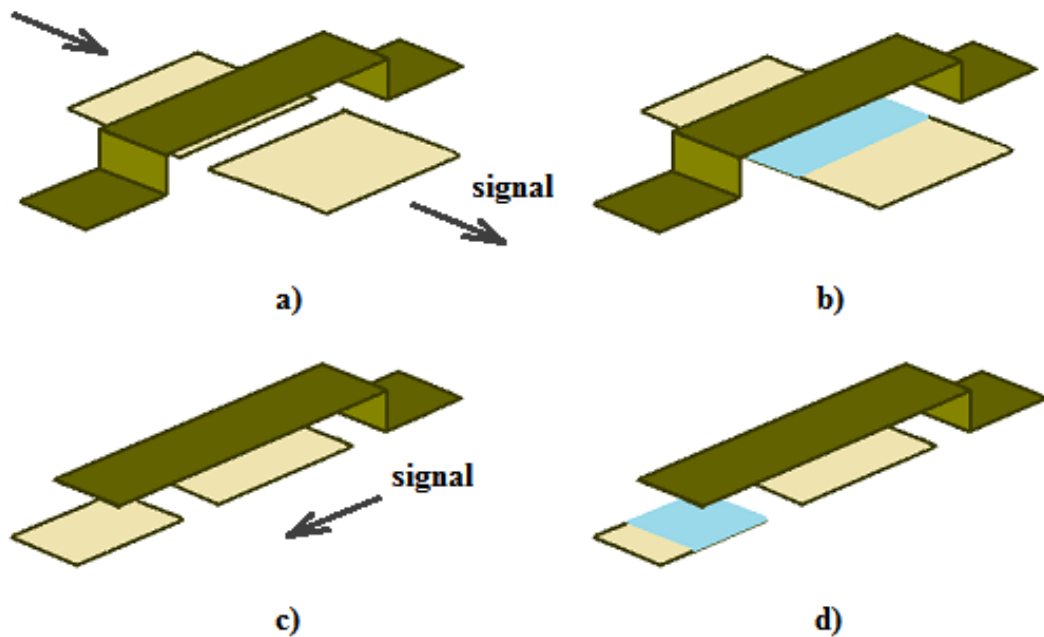


**Figure 2.7** Switch types: (a) shunt metal-contact switch (b) shunt capacitive switch (c) series metal-contact switch (d) series capacitive switch

Last but not least, for RF MEMS switches, there are four actuation mechanisms that are electrostatic, magneto static, thermal and piezoelectric. Electrostatic actuation is most

preferred method among these, because of zero power consumption, having almost no mass and relatively being not sensitive to acceleration [54].

## 2.4 Fabrication and Packaging of RF MEMS

The manufacture of RF MEMS devices is done in clean room laboratories, using generally chemical and physical operations with super sensitive machines. Sometimes aluminum, chromium, copper and titanium but frequently gold is used as metal material for structure. From this point of view, it may be seemed as an expensive technology but since they are extremely small devices, their unit costs are still acceptable.

RF MEMS switches are manufactured on silicon or glass substrates that are rounded and generally 4-6-8 inches wide. Silicon is generally suitable to use for electronics and also from mechanical perspective, it is reliable in long term due to its low fatigue level, furthermore it is an inexpensive material.

Number	Step Name	Layer Name	Material Name	Thickness	Mask Name	Photore	Depth
0	Substrate	Substrate	SILICON_100	5	substrate		
1	LPCVD Silicon Nitride Deposition	passivation	SI3N4	0.1			
2	LPCVD Polycrystalline Silicon Deposition	electrode	POLYSILICON	0.2			
3	Polysilicon and OXIDE Patterning: RIE Plasma Etch				mask1	-	
4	Sacrificial Polyimide Deposition	sacrificial	POLYIMIDE	0.3			
5	Polyimide Patterning: RIE Plasma Etch				mask2	-	
6	Polyimide Patterning: RIE Plasma Etch				mask3	-	0.1
7	Conformal Shell	mechanical	Gold_35_044	1.6			
8	Polyimide Patterning: RIE Plasma Etch				substrate	-	0.6
9	Release		POLYIMIDE				
10	Polyimide Patterning: RIE Plasma Etch				mask4	-	

**Figure 2.8** Building steps of simulation program

Metals can be deposited by electroplating, evaporation, and sputtering processes. Electroplating is to use electric current to form a metal coating on an electrode. In evaporation, material is evaporated thermally or electrically and deposited in a vacuum area and lastly in sputtering, material stays as ion beam over the substrate and leave atoms to the substrate for deposition, in other words metal is atomized or pulverized.

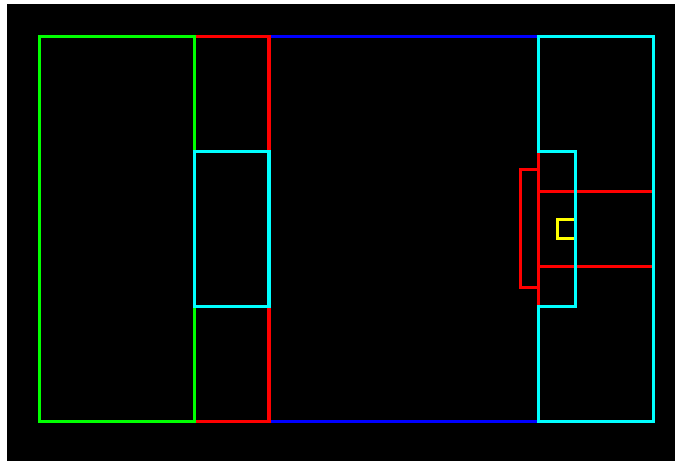


**Figure 2.9** Mask layers that used in fabrication

To build and analyze this model, different masks are used in an order and a proper mask must be added to the models as shown in Figure 2.9. With different layers of masks, different deposition and etching steps are done in Coventor (see Figure 2.8).

Designing the RF MEMS devices on the substrate is possible thanks to photolithography method in which a photoresist layer that consist of photosensitive material added (spread centrifugal) over deposited metal layer and exposed to a radiation (generally light with adjustable wavelengths) through a mask. In this way, the pattern that imprinted on the mask is transferred to the metal layer via contact aligner, and then photoresist layer is cleaned with a solution except the exposed areas. Finally, the dissolvent of the metal is applied to the metal layer in a proper time which is called wet etching (dry etching method is also available for this) and thus desired metal form is obtained. These steps may be repeated several times with different masks in order to get the desired structure. Figure 2.10 shows the basic steps of RF MEMS switch fabrication and Figure 2.8 shows the manufacturing steps of Coventor software program which uses real time manufacturing method before analyzing the performance of the MEMS devices.

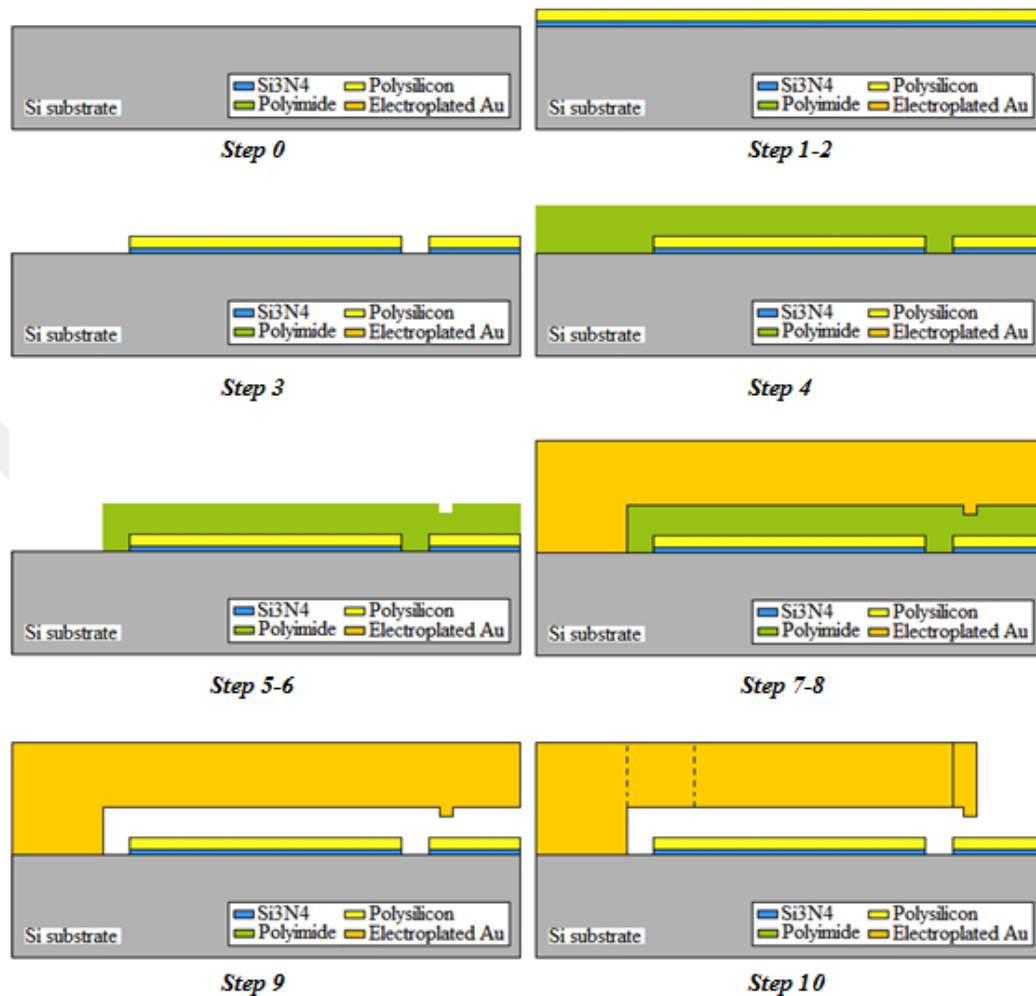
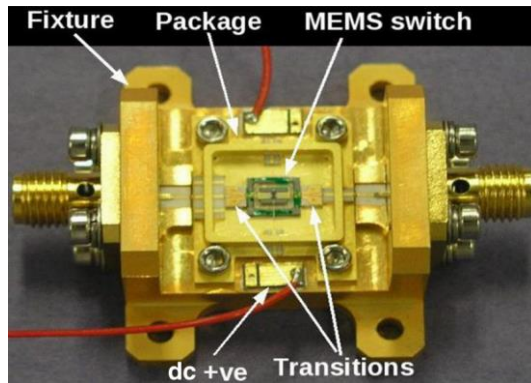
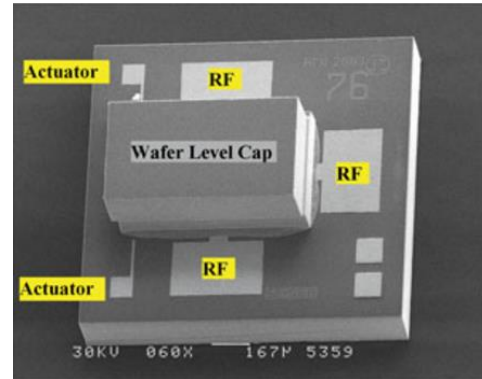


**Figure 2.10** Schematic view of RF MEMS switch fabrication steps

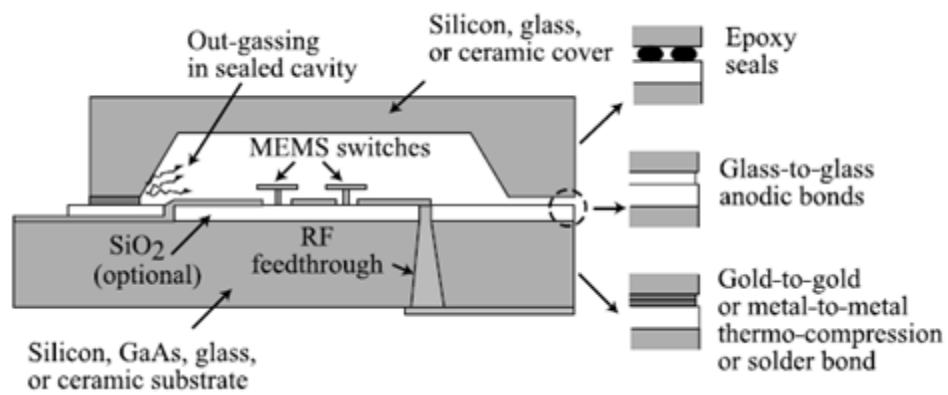
In manufacturing process, generally hundreds of RF MEMS switches are located together on silicon wafer so each switch must be diced before usage. After that, diced switches must be covered properly with hermetic lock for protection and reliability which is called packaging. Although the packaging is generally assumed as the most expensive process, it is vitally important especially for commercial use because dust and humidity, the most common enemies of the RF MEMS devices, can easily effect the performance of the micro devices in short and long term. It also removes heat and ensures substantiality.



(a)



(b)



(c)

**Figure 2.11** (a) and (b) real pictures of packaged switches (c) on-wafer hermetic packaging of mems switches [55-56]

For the packaging, silicon, ceramic or glass covers are preferred and the inner atmosphere is filled with nitrogen, argon or dry-air. To place the top cover, carrier columns must be designed on substrate. Only the transmission line can go in and out of the package [3]. There are two examples of real packaged switches in the figure below.

# CHAPTER 3

## MECHANICAL PARAMETERS OF A CANTILEVER BEAM TYPE RF MEMS SWITCH

### 3.1 Stiffness of Cantilever Beam

One of the most important features while analyzing characteristics of RF MEMS switch is pull\_in voltage. It is the value of the applied voltage at the exact time of collapse instant. In RF MEMS world, collapsing of the structure - in this case cantilever beam - refers to the switching. To determine the pull\_in voltage, it is essential to understand the mechanical stiffness concept.

#### 3.1.1 Deflection under Electrical Actuation

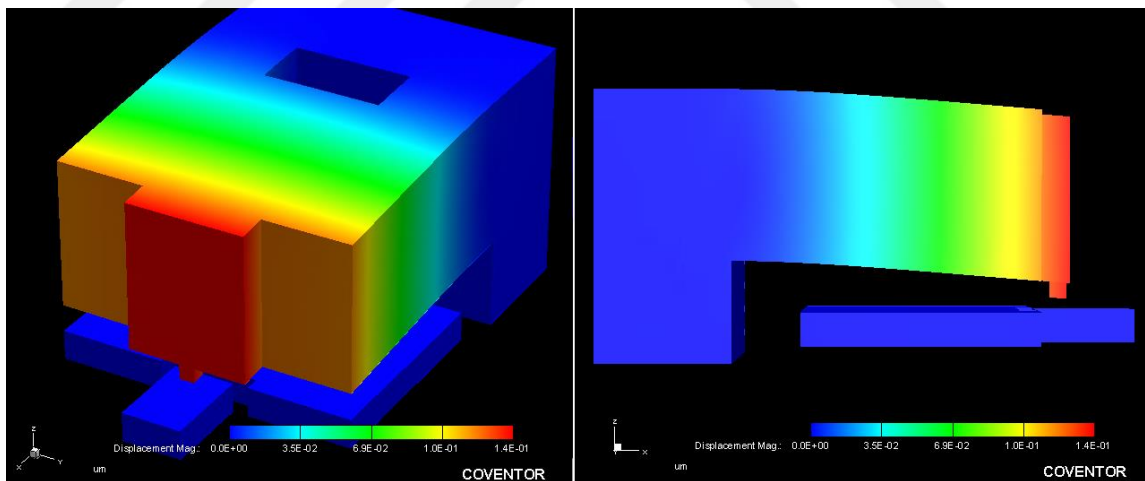


**Figure 3.1** Three times exaggerated isometric view and side view of a bended cantilever beam under actuated voltage

To obtain the spring constant of the cantilever beam, calculation of deflection is the first step. In order to find the deflection, it is also needed to be determined a stabile



concentrated or distributed load. However, in electrically actuating situation, there is no such a load type as its reasons are mentioned in Section 2. Hence, to get to the main point, only the load distribution at the exact collapse time is taken into consideration in order to obtain the deflection and thereby stiffness (Figure 3.1). It means, each position during the motion gives different load distribution and each different load distribution gives different spring constant. Gabriel M. Rebeiz and Chirag Patel called the situation that represents collapse instant as actuation stiffness [7].

The deflection at the end of the cantilever beam just before the collapse time is called maximum tip deflection and can be found via distributed load. The consisted distributed load is calculated using electrostatic force formula which comes from parallel plate capacitance theory [3].

$$F_e = -\frac{1}{2} \frac{\epsilon_0 W w V^2}{g^2} \quad (3.1)$$

Here,  $F_e$  is sum of the distributed load,  $V$  is the applied voltage,  $W$  is length of the actuation pad,  $w$  is width of the cantilever beam and  $g$  is gap between two metals (cantilever and actuation pad). This equation only gives the correct results in parallel situation which means that two metal plates remain parallel during the motion. However, when a cantilever beam's fixed end stays steady, the free end bends under an applied voltage which means there is no parallelism. To use this equation for a cantilever beam, beam must be divided into finite parallel elements and the electrostatic force must be calculated for each element and then those finite elements must be integrated.

As it can be seen from the electrostatic force equation, the distributed load is mostly related with the gap, because when the geometry of the structure and the applied voltage remain stationary, the gap between the beam and the pad is changing continuously. Changing of the shape and the amount of the distributed load and the gap continuously

until the collapse time is an explicit indicator of why actuation stiffness concept is necessary.

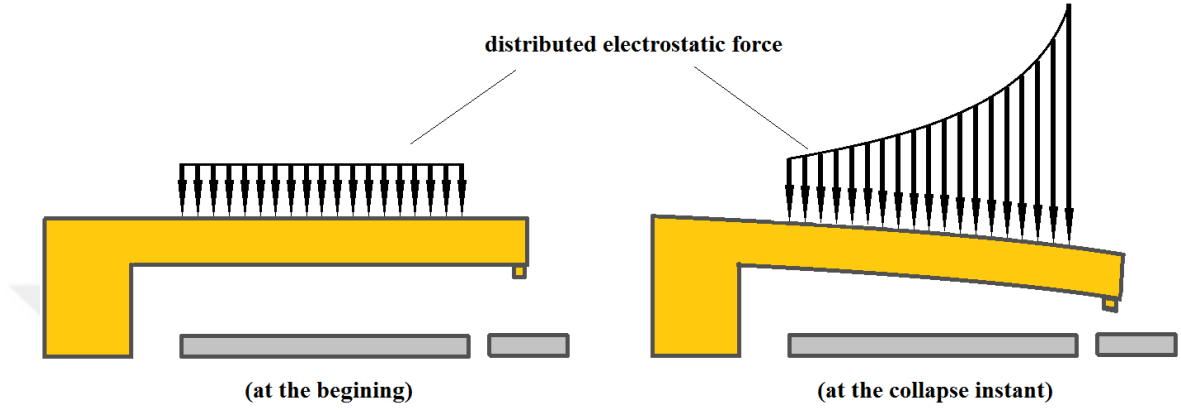


**Figure 3.2** Side view of an actuated beam

The applied voltage and the shape of the bended cantilever are needed to calculate the distributed load and thereby to obtain the actuation spring constant. Two shapes of the cantilever beam with consisted distributed load, at the beginning and just before the collapse instant are shown in Figure 3.2, respectively. In addition to this, from the simulation results in Section 3.3, it is obvious that the maximum tip deflection  $d_{\max}$  of different beams under same conditions is around 0.5 times the initial gap  $g_0$  (see Table 3.3). These two data show that the distributed load can be calculated as if it is a linear shaped cantilever beam. As a result, maximum tip deflection of the cantilever beam is assumed as the half of the initial gap.

$$d_{\max} = \frac{g_0}{2} \quad (3.2)$$

Shape of the consisted distributed load is simplified as linear for convenience. (see Figure 3.3). This assumption is based on optimization calculation that is done to find same distributed load. In other words, total load is not changing after linearization.

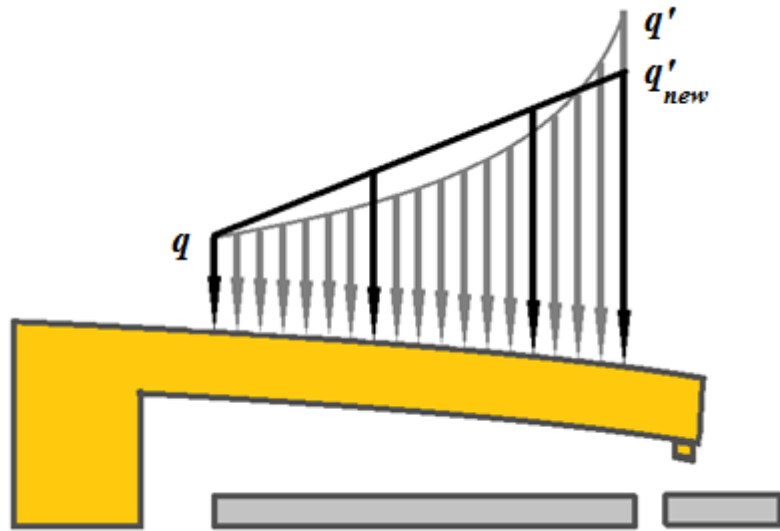


**Figure 3.3** The distributed load is simplified as linear

The voltage which causes the motion of cantilever beam is applied by an underlying actuation pad which is represented in Figure 3.2. The distributed load occurs only in alignment of this actuation pad. As shown in Figure 3.4 (a), the distributed load is divided into two parts to apply superposition method.

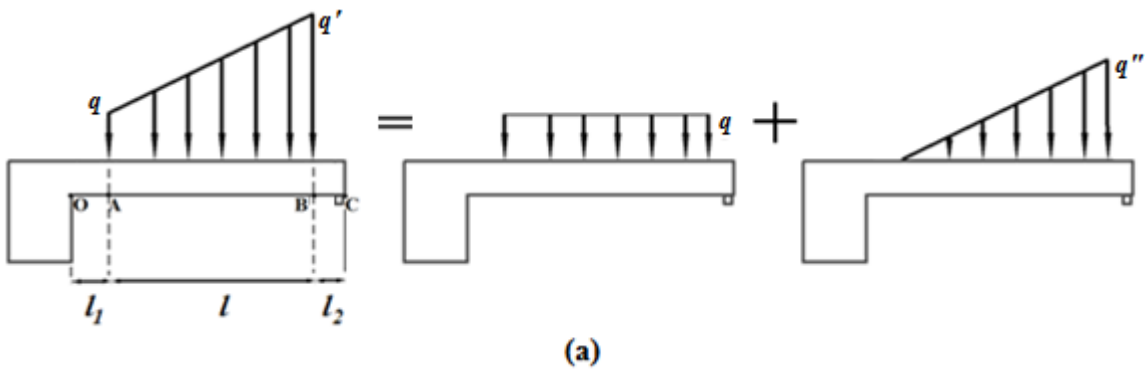


**Figure 3.4 (a)** Separated distributed load

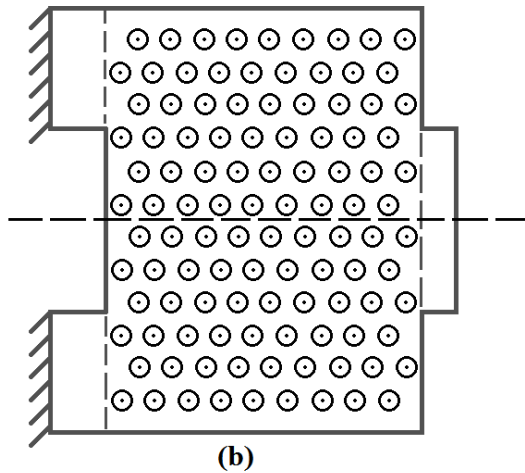


**Figure 3.4 (b)** The top view of distributed load and the cutting line

The top view of the beam with distributed load can be seen from Figure 3.4 (b). Since there will be no difference for displacement result, beam is divided into two parts from half of the width in order to decrease the number of unknown variables. Then, the distributed load must be turned into concentrated load to perform the calculations. This process is shown in Figure 3.5. After that, superposition method is used to calculate the tip deflection.

In the superposition method, beam must be separated from critical points like moment of inertia changes or applied load changes. While this cantilever beam subjected to a distributed load at AB part, OA and BC parts have no load. Besides, the inertia moment of OA part consists of summation of the different inertia moments due to different cross-section dimensions.

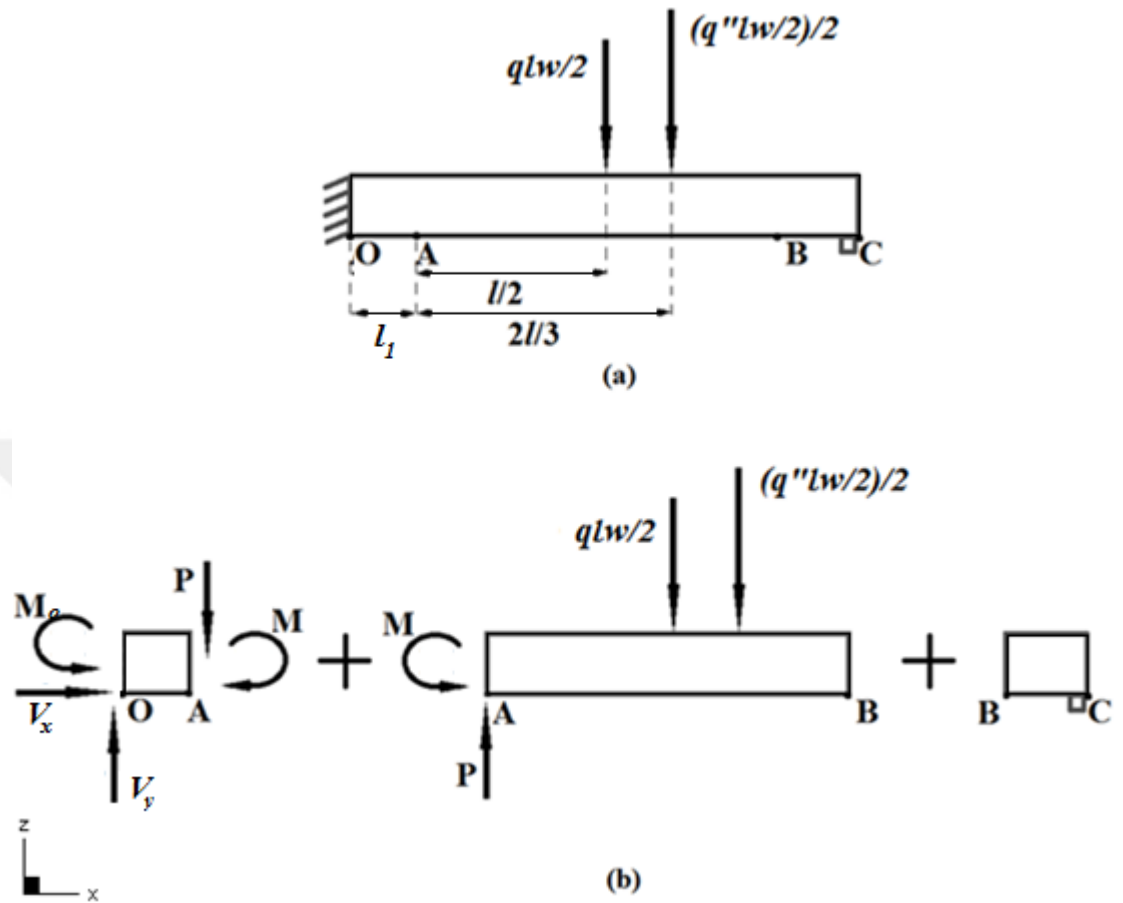


**Figure 3.5** The concentrated loads and the superposition method

For OA part:

The shear force and the total moment at point A are found, displacements and the angles of bending can be obtained using mechanics of material equations [59],

$$P = \frac{qlw}{2} + \frac{q''lw}{4} \tag{3.3}$$

where, P is the shear formula that occurs at point A.

$$M = \frac{qlw}{2} \frac{l}{2} + \frac{q''lw}{4} \frac{2l}{3} \tag{3.4}$$

where,  $M$  is the bending moment at point A. Then, the deflection at A due to the force  $P$  is found as follows:

$$\delta_1 = \frac{Pl_1^3}{3EI_{OA}} \quad (3.5)$$

Deflection due to the moment  $M$  is:

$$\delta_2 = \frac{Ml_1^2}{2EI_{OA}} \quad (3.6)$$

Slope due to the force  $P$  is:

$$\theta_1 = \frac{Pl_1^2}{2EI_{OA}} \quad (3.7)$$

Slope due to the moment  $M$  is:

$$\theta_2 = \frac{Ml_1}{EI_{OA}} \quad (3.8)$$

*For AB part:*

The total forces in  $z$  direction and total moment at point A must be calculated before cutting the AB part from an  $x$  point.

$$\uparrow^+ \sum F_z = 0$$

$$P = \left(ql + \frac{ql}{2}\right) \frac{w}{2} \quad (3.9)$$

$$\circlearrowleft^+ \sum M_A = 0$$

$$M_A = \left( ql \frac{l}{2} + \frac{q''l}{2} \frac{2l}{3} \right) \frac{w}{2} = l^2 \left( \frac{q}{2} + \frac{q''}{3} \right) \frac{w}{2} \quad (3.10)$$

Now, the AB part is cut from an  $x$  point (Figure 3.6) to obtain its partial deflection.

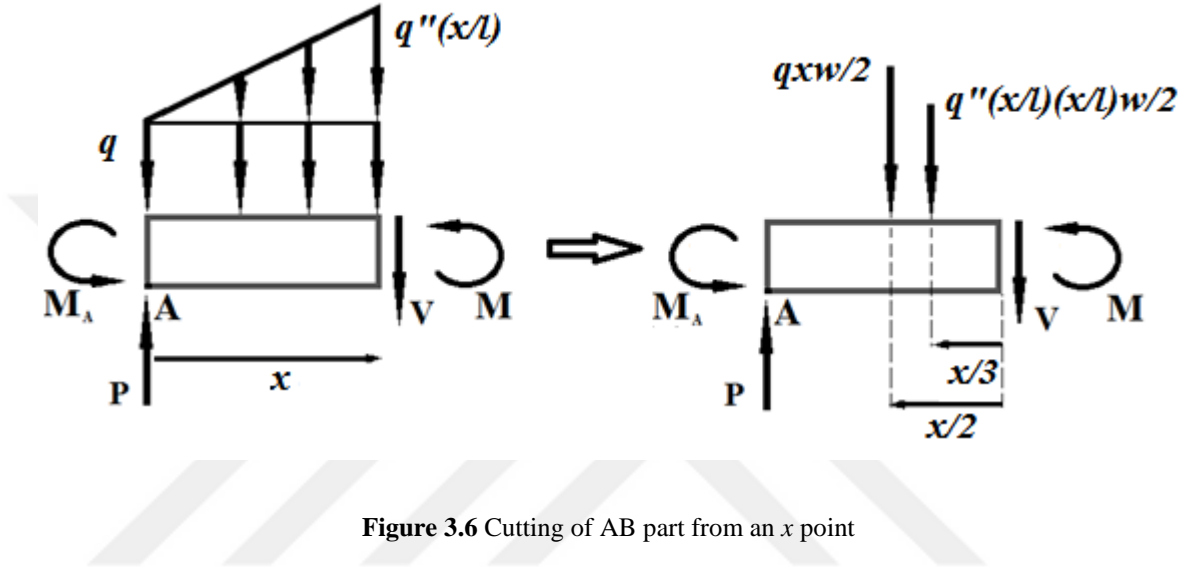


Figure 3.6 Cutting of AB part from an  $x$  point

$$\sum M_x = 0$$

$$M + M_A - Px + qx \frac{x}{2} + \frac{q''x^2}{2l} \frac{x}{3} = 0 \quad (3.11)$$

Substituting the values in Eq. 3.11, it gives;

$$M = \frac{-l^2(3q + 2q'')}{6} + \left( ql + \frac{q''l}{2} \right) x - \frac{3qx^2}{6} - \frac{q''x^3}{6l} \quad (3.12)$$

Also, the elastic equation is known as;

$$M = EI_{AB} \frac{d^2z}{dx^2} \quad (3.13)$$

The boundary conditions are known as,

$$\text{at } x=0; \frac{dz}{dx} = 0 \text{ and } z = 0.$$

Hence, Eq. 3.12 and Eq. 3.13 are solved with the boundary conditions,

$$EI_{AB} \frac{d^2z}{dx^2} = \frac{[-l^2(3q + 2q'') + (6ql + 3q''l)x - 3qx^2 - \frac{q''x^3}{l}]}{6} \quad (3.14)$$

From Equation 3.14, the deflection due to the distributed load at the end of the part AB is found for  $x=l$  as follows,

$$\delta_3 = \frac{l^4(15q + 11q'')}{120EI_{AB}} \cdot \frac{w}{2} \quad (3.15)$$

$\theta_3$  which occurs resulted from the distributed load at the end of the part AB is also obtained from Eq. 3.14,

$$\frac{dz}{dx} = \frac{\left[ \frac{-l^2(3q + 2q'')x}{6} + \frac{(6ql + 3q''l)}{12}x^2 - \frac{qx^3}{6} - \frac{q''x^4}{24l} \right]}{EI_{AB}} \quad (3.16)$$

Eq. 3.16 is taken from derivation operations of part AB and solving for  $\theta_3$ ,

$$\theta_3 = \frac{l^3}{24EI_{AB}} (4q + 3q'') \frac{w}{2} \quad (3.17)$$

The deflection due to the angles  $\theta_1 + \theta_2$  is,

$$\delta_4 = (\theta_1 + \theta_2)l \quad (3.18)$$



For BC part:

The angles coming from equations 3.7, 3.8 and 3.17 cause a deflection for BC the last part of the beam and it is found from following relation:

$$\delta_5 = (\theta_1 + \theta_2 + \theta_3)l_2 \quad (3.19)$$

Additional Part:

Since the beam was dimidiated, the anchor of new beam is not located in symmetric for the part that the load is applied. It causes an additional bending towards the free part that does not have an anchor in its line. However, it would be wrong to calculate this bending effect by considering the divided beam. This situation must be considered as fixed-simply supported beam model and be added to the total deflection. Fig 3.7 shows this additional situation.

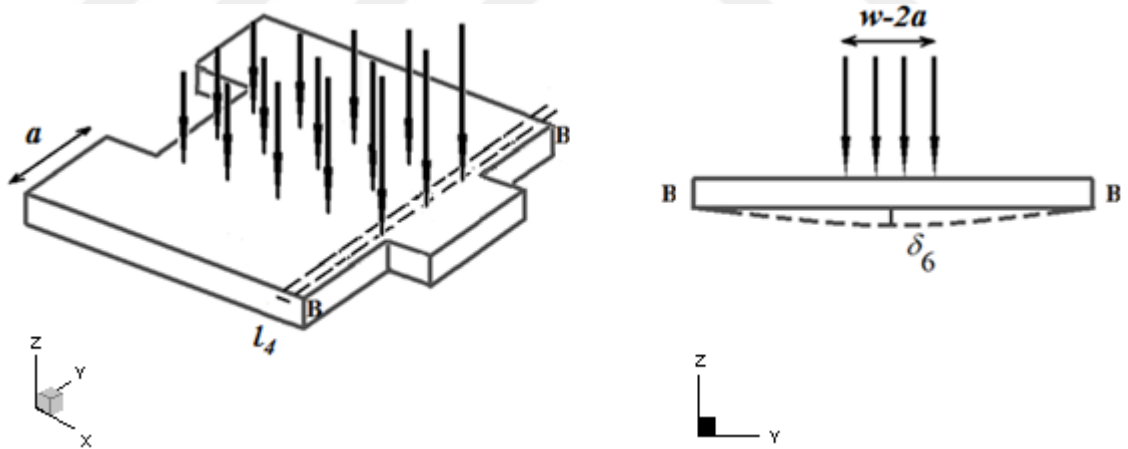


**Figure 3.7** Additional deflection at the center due to the hole

The right one of the Figure 3.7 shows the front view of the beam and this additional deflection formula  $\delta_6$  comes from mechanics [60]. The distributed load is taken into consideration as concentrated load.

$$\delta_6 = \frac{q_B(w-2a)l_4w^3}{48EI_{BB}} \quad (3.20)$$

where,  $q_B$  is the unit load at point B which equals to  $q'$  and  $l_4$  is the width of the cross-section of BB line.

As all deflection values coming from different parts are obtained, the total tip deflection is found by equations 3.5, 3.6, 3.15, 3.18, 3.19, 3.20 as follows,

$$\sum \delta = \delta_1 + \delta_2 + \delta_3 + \delta_4 + \delta_5 + \delta_6 \quad (3.21)$$

The moment of inertia of part OA, AB, AC and BB in which the length equals to the width and the width is  $l_4$ , respectively [59]:

$$I_{OA} = \frac{at^3}{12} \quad (3.22)$$

$$I_{AB} = I_{AC} = \frac{wt^3}{24} \quad (3.23)$$

$$I_{BB} = \frac{l_4t^3}{12} \quad (3.24)$$

where,  $t$  is thickness of the beam.

Geometric dimensions of the designed beam are given in Table 3.1.

**Table 3.1** The geometry variables in  $\mu m$  unit for cantilever beam model

$L$	$l_1$	$l$	$l_2$	$w$	$a$	$t$	$g_0$	$E_{gold}$
10	2	7	1	10	3	1	0.3	35 [GPa]

The effective Young's modulus equivalent to the plate modulus that is given as  $E/(1-\nu)^2$  for wide beams ( $w \geq 5t$ ) where  $\nu$  is the Poisson's ratio here and equals to 0.44 for gold. For more narrow beams ( $w < 5t$ ), Young's modulus is basically taken without dividing into Poisson ratio [61].

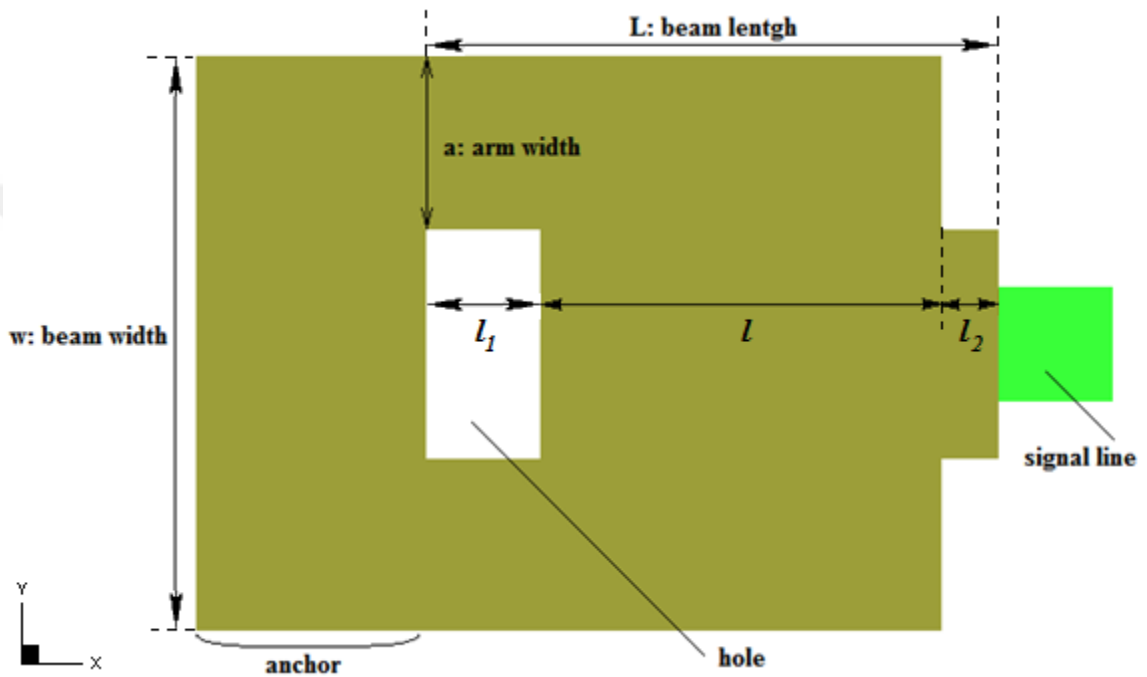


**Figure 3.8** Dimensions from top view of the beam

With the moments of inertia, the total tip deflection from Eq. 3.21 can be found as depended on  $q$  and  $q'$  via MATLAB.

$$\sum \delta = 2.38 \times 10^{-13} q'' + 3.62 \times 10^{-13} q + 8.36 \times 10^{-9} \mu m \quad (3.25)$$

### *Finding Unit Loads*

In order to find the amount of the distributed load, electrostatic force  $F_e$  formula is used. Since  $F_e$  formula gives the total distributed load, it is needed to be divided to area because

all deflection calculations are performed according to the load per area thus far. (Eq. 3.29)  
 The beam shape at collapse (pull\_in) instant and the geometry for  $q$  and  $q'$  are shown in Figure 3.9.

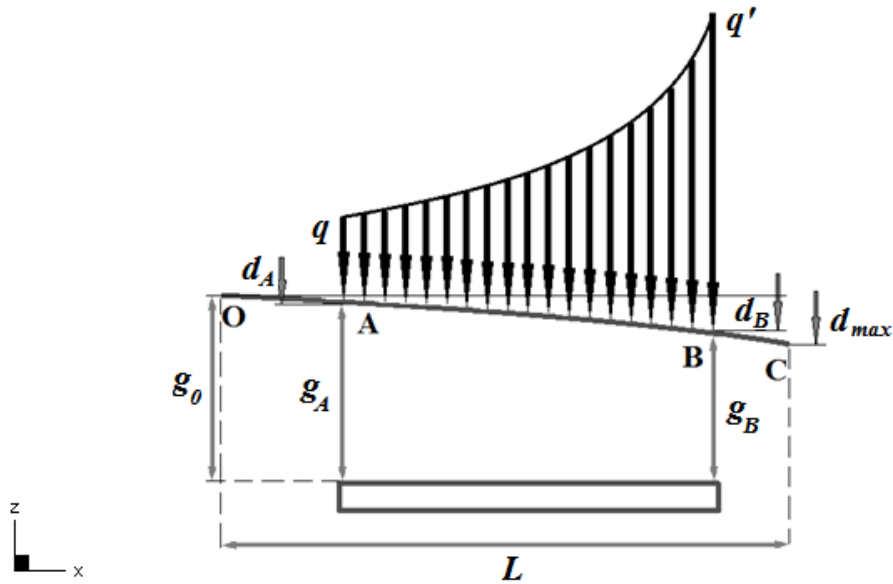


**Figure 3.9** Calculation for  $q$  and  $q'$

From the similarity of the triangle,

$$\frac{d_{\max}}{L} = \frac{d_A}{l_1} = \frac{d_B}{l_1 + l} \quad (3.26)$$

The gap at point A,

$$g_A = g_0 - d_A \quad (3.27)$$

The gap at point B,

$$g_B = g_0 - d_B \quad (3.28)$$

Herein,  $g_A$  and  $g_B$  are the gaps,  $d_A$  and  $d_B$  are deflection of point A and B which are the places that actuation pad starts and ends at the collapse instant respectively. From Eq. 3.1 and Eq. 3.2, the unit loads at point A and B are found as follows,

$$q = \frac{F_e}{w.W} = \frac{0.5\varepsilon_0 V^2}{g^2} \text{ N/m}^2 \quad (3.29)$$

$$q_A = q = 0.135 \times 10^6 \text{ N/m}^2 \quad (3.30)$$

$$q_B = q' = 0.403 \times 10^6 \text{ N/m}^2 \quad (3.31)$$

$$q'' = q' - q \text{ N/m}^2 \quad (3.32)$$

Actuation voltage is 50.56 V which is taken from simulation results to get a distributed load value. Also, a small simplification is done for distributed load, so  $q'$  is the real unit load value of point B. However,  $q'$  should be taken 0.1 times smaller for being linear as represented in Figure 3.3. (New  $q' = 0.363 \times 10^6 \text{ N/m}^2$ ). If Eq. 3.22, 3.23, 3.24,  $q$  and the simplified  $q'$  are substituted into Eq. 3.21, the total maximum displacement can be found as follows,

$$\sum \delta = 0.112 \text{ } \mu\text{m} \quad (3.33)$$

Hereby, the maximum tip deflection of the cantilever is found exactly, but the real issue is how to obtain the spring constant and pull\_in voltage. There are two possible attitudes to get the actuation spring constant from this point. One of them is dividing the total distributed load into the tip deflection. In other respects, the second way offers to apply an imaginary concentrated load at the center of gravity of the distributed load and to obtain

its deflection formula and equalize it to Eq. 3.33. From this equation, if the concentrated load is extracted and divided into the deflection, the spring constant is found.

### 3.1.2 Natural Spring Constant

Before analyzing the actuation spring constant, it would be helpful to obtain the natural spring constant. In mechanical engineering, a concentrated load applied to the free end of the cantilever to obtain the spring constant as is known, but natural stiffness is found by applying a stable uniform distributed load to the beam for RF MEMS switches [7]. It is useful to get an idea easily before starting to analyze the main characteristics. It is clear that the spring constant is only related to the geometry except the load type. To find the natural stiffness of the cantilever beam, there is no need to know a voltage or deflection values,

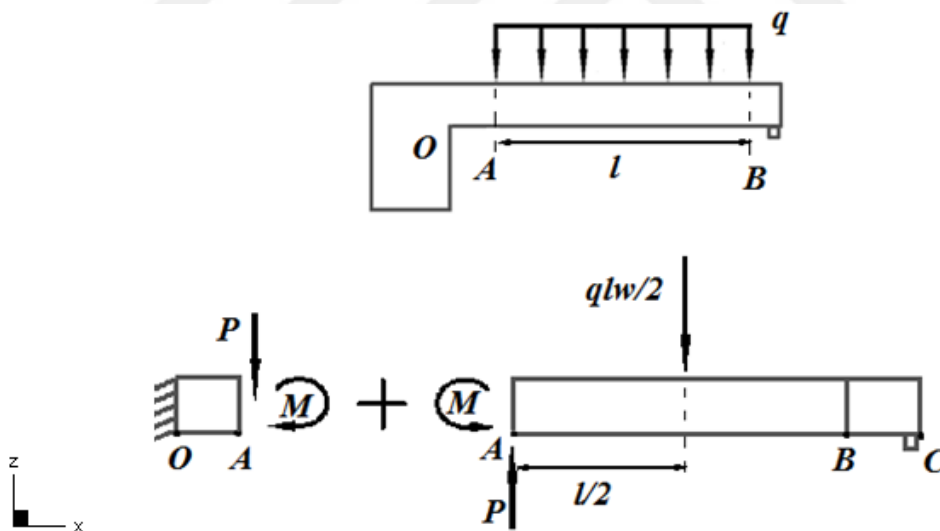


Figure 3.10 Superposition for natural stiffness

The shear force and the bending moment at point A [59],

$$P = \frac{qlw}{2} \quad (3.34)$$

$$M = P \frac{l}{2} \quad (3.35)$$

Deflection due to the force P,

$$\delta_1 = \frac{Pl_1^3}{3EI_{OA}} \quad (3.36)$$

Deflection due to the moment M,

$$\delta_2 = \frac{Ml_1^2}{2EI_{OA}} \quad (3.37)$$

Slope due to the force P,

$$\theta_1 = \frac{Pl_1^2}{2EI_{OA}} \quad (3.38)$$

Slope due to the moment M,

$$\theta_2 = \frac{Ml_1}{EI_{OA}} \quad (3.39)$$

Deflection due to the angles  $\theta_1$  and  $\theta_2$ ,

$$\delta_4 = (\theta_1 + \theta_2)(l + l_2) \quad (3.40)$$

Deflection due to the distributed load,

$$\delta_3 = \frac{ql^4(w/2)}{8EI_{AB}} \quad (3.41)$$

Slope due to the distributed load,

$$\theta_3 = \frac{ql^3(w/2)}{6EI_{AB}} \quad (3.42)$$

Deflection due to the angle  $\theta_3$ ,

$$\delta_5 = \theta_3 \left( \frac{l}{2} + l_2 \right) \quad (3.43)$$

And the total displacement and thereby natural spring constant are found respectively,

$$\sum \delta = \delta_1 + \delta_2 + \delta_3 + \delta_4 + \delta_5 \quad (3.44)$$

$$k_{nat} = \frac{qlw}{\sum \delta} = 167.7 \frac{N}{m} \quad (3.45)$$

### 3.1.3 Actuation Spring Constant

M. Rebeiz claims that actuation stiffness is found by dividing the distributed load into deflection directly [3]. Since  $q$  and  $q''$  are known, the electrostatic force and actuation stiffness become:

$$F_e = lw \left( q + \frac{q''}{2} \right) \quad (3.46)$$

$F_e$  is found  $17 \mu m$ , and it must be divided into total deflection to find actuation spring constant,

$$k_{act} = \frac{F_e}{\sum \delta} = 153.2 \frac{N}{m} \quad (3.47)$$



From mechanical aspect, it is a little arguable approach that dividing the total distributed load directly into the deflection, still, Rebeiz derived a pull\_in voltage formula which uses this stiffness type and it gives good results. This subject is analyzed in Section 3.2.1.

Additionally, a different approach is to apply a concentrated load at the center of gravity of the distributed load. Figure 3.12 shows the free body diagram of the beam that divided into two like deflection calculation. That is why half of the concentrated load is used.

Since there is no distributed load, it is not necessary to take bending to the free side into consideration.

Since  $q$  and  $q''$  are known, the center of gravity of the distributed load can be found easily as is shown in the figure below,

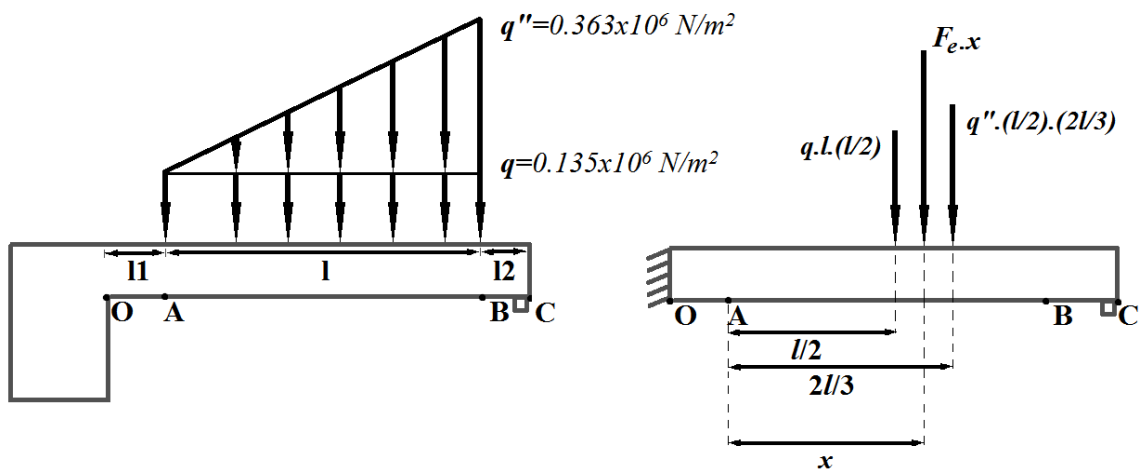


**Figure 3.11** Finding of the center of gravity of the distributed load

To use this method,  $x$  is found 0.6 times the length. Thus, the place, where the concentrated load is applied, is determined and the displacement can be found.

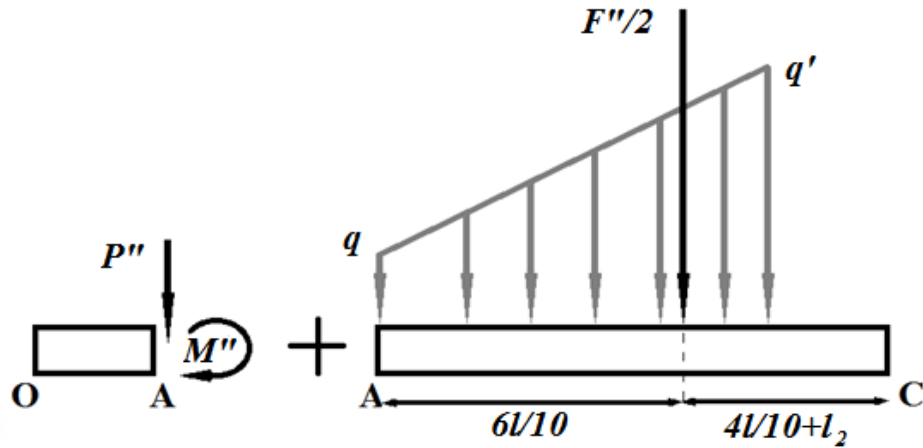


Figure 3.12 Concentrated load at the center of gravity

In Figure 3.12,  $F''$  shows the concentrated load at the center of gravity. Since the beam is divided into two parts, only half of this load is taken into account. In order to differentiate the shear force and bending moment for this solution, they are shown with double prime and they are calculated with same principles [59],

$$P'' = \frac{F_{mid}}{2} \quad (3.48)$$

$$M'' = \frac{F_{mid}}{2} \frac{6l}{10} \quad (3.49)$$

Deflection due to the force  $P''$ ,

$$\delta_1'' = \frac{P'' l_1^3}{3EI_{OA}} \quad (3.50)$$

Deflection due to the moment  $M''$ ,

$$\delta_2'' = \frac{M'' l_1^2}{2EI_{OA}} \quad (3.51)$$

Slope due to the force  $P''$ ,

$$\theta_1'' = \frac{P'' l_1^2}{2EI_{OA}} \quad (3.52)$$

Slope due to the moment  $M''$ ,

$$\theta_2'' = \frac{M'' l_1}{EI_{OA}} \quad (3.53)$$

Deflection due to the angles  $\theta_1''$  and  $\theta_2''$  at the free end of the beam,

$$\delta_3'' = (\theta_1'' + \theta_2'')(l + l_2) \quad (3.54)$$

Deflection due to the concentrated load at the center of gravity,

$$\delta_4'' = \frac{F_{mid}}{2} \left( \frac{6l}{10} \right)^3 \frac{1}{3EI_{AC}} \quad (3.55)$$

Slope due to the concentrated load at the center of gravity,

$$\theta_3'' = \frac{F_{mid}}{2} \left( \frac{6l}{10} \right)^2 \frac{1}{2EI_{AC}} \quad (3.56)$$

Deflection due to the angle  $\theta_3''$ ,

$$\delta_5'' = \theta_3'' \left( \frac{2l}{12} + l_2 \right) \quad (3.57)$$

Total tip deflection is,

$$\sum \delta'' = \delta_1'' + \delta_2'' + \delta_3'' + \delta_4'' + \delta_5'' \quad (3.58)$$

When the total tip deflection that is given by Eq. 3.58 is equalized to Eq. 3.33 the imaginary concentrated load at the center of the gravity of the distributed load  $F_{mid}$  is found. If this force is divided into displacement, the spring constant can be found for second actuation stiffness approach as follows.

$$F_{mid} = 19.1 \mu N \quad (3.59)$$

$$k_{act2} = 171 \frac{N}{m} \quad (3.60)$$

These two spring constants are being compared in Section 3.2.2 to find the pull\_in voltage.

### 3.1.4 Release Spring Constant

Release stiffness is important to obtain the collapse voltage of the beam. To determine it, a concentrated load at the free end is applied to the cantilever beam and its deflection equation is obtained. Figure 3.13 shows the detail of this method. Shear force and bending moment are shown with prime.

$$P' = \frac{F_{end}}{2} \quad (3.61)$$

$$M' = \frac{F_{end}}{2}(l + l_2) \quad (3.62)$$

where,  $F_{end}$  is the concentrated load that occurs at the end as the beam wants to get back to the initial equilibrium position. Deflection due to the force  $P'$ ,

$$\delta_1' = \frac{P'l_1^3}{3EI_{OA}} \quad (3.63)$$

Deflection due to the moment  $M'$ ,

$$\delta_2' = \frac{M'l_1^2}{2EI_{OA}} \quad (3.64)$$

Slope due to the force  $P'$ ,

$$\theta_1' = \frac{P'l_1^2}{2EI_{OA}} \quad (3.65)$$

Slope due to the moment  $M'$ ,

$$\theta_2' = \frac{M'l_1}{EI_{OA}} \quad (3.66)$$

Deflection due to the angles  $\theta_1'$  and  $\theta_2'$ ,

$$\delta_3' = (\theta_1' + \theta_2')(l + l_2) \quad (3.67)$$

Deflection due to the concentrated load at the end of the beam,

$$\delta_4' = \frac{\frac{F_{end}}{2}(l + l_2)^3}{3EI_{AC}} \quad (3.68)$$

Total deflection is,

$$\sum \delta' = \delta_1' + \delta_2' + \delta_3' + \delta_4' \quad (3.69)$$

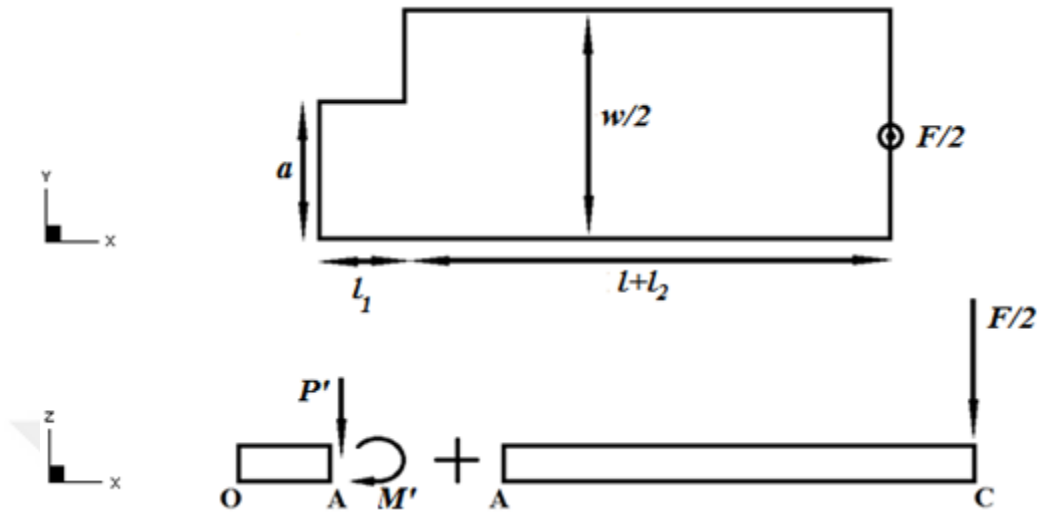


**Figure 3.13** Concentrated load is at the end for release stiffness

When the Eq. 3.69 is equalized to Eq. 3.33 the concentrated load at the end of the beam  $F_{end}$ , which is the load that occurs at the collapse instant, is found and if it is divided into displacement, the release spring constant can be found.

$$F_{end} = 9.1 \mu N \quad (3.70)$$

$$k_{rel} = 81.9 \frac{N}{m} \quad (3.71)$$

This spring constant only shows the release situation during the motion between the beginning and the contact time, not beyond. After the contact situation, a different solution is needed due to the changing beam shape. Section 3.2.1 is analyzing this subject.

### 3.2 Calculations of Other Switch Parameters

Stiffness is the base parameter for all calculations of RF MEMS switch, that is why it is studied first. Other important mechanical parameters like pull\_in voltage, contact force, release force and switching time are analyzed in Section 3.2.

### 3.2.1 Pull\_In Voltage

The importance of the pull\_in voltage concept is discussed in Section 2 and Section 3.1. In this section, how to obtain the pull\_in voltage is examined. G. M. Rebeiz formed a basic formula for a basic electrically actuated cantilever beam situation. Although, every design needs a different calculation because of different geometry and different load type, this formula is helpful to get a rough estimate for the voltage that collapses the beam and thereby the switching [3].

$$V_p = V(2g_0/3) = \sqrt{\frac{8k}{27\varepsilon_0 Ww}} g_0^3 \quad (3.1)$$

According to the spring constant values found in the previous part, this formula gives different results by comparing with the real value 50.56 V. The pull\_in voltages that are obtained from this formula using  $k_{end}$ ,  $k_{mid}$  and  $k_{act}$  are given below respectively.

$$V_{pull\_in(end)} = 32.5 \text{ V} \quad (3.72)$$

$$V_{pull\_in(mid)} = 46.9 \text{ V} \quad (3.73)$$

$$V_{pull\_in(act)} = 44.5 \text{ V} \quad (3.74)$$

As it is seen, the closest result to the real value is obtained using  $k_{mid}$ , this shows that the spring constant, which is in the Rebeiz's pull\_in voltage formula, is obtained by dividing the total distributed load into the deflection. Here, another empirical formula for pull\_in voltage can be derived using  $k_{end}$  and  $k_{mid}$  but it wouldn't give exact result for varied designs.

$$V_{pull\_in\_cht} = \sqrt{\frac{k_{mid}}{3\varepsilon_0 Ww}} g_0^3 \quad (3.75)$$

With this formula, pull\_in voltage is found 49.8 V. It should be kept in mind that, the spring constant that is used in this derived equation is obtained by the center of gravity method. For actuation stiffness a different equation can be derived too,

$$V_{pull\_in\_cht} = \sqrt{\frac{k_{act}}{2.5\epsilon_0 W w}} g_0^3 \quad (3.76)$$

However, these empiric formulas (Eq. 3.75 and Eq. 3.76) are obtained with considering the true results which are coming from simulation. Therefore, more experiments with different designs from literature must be performed to verify them.

Instead of using these formulas, it is possible to develop a solution via MATLAB for a better approach to real value. Moreover, as mentioned in Section 1, there will be two different pull\_in voltage solutions for two different spring constant approaches.

It can be seen from Figure 3.2 that the shape of the beam is almost like an inclined plane because the gap over beam length ratio is too small (gap: 0.3  $\mu m$ , length: 10  $\mu m$ ). Because of the fact that the bended beam's shape is assumed linear till the collapse instant. In order to calculate the total electrostatic force and reaction force on the purpose of investigate pull\_in voltage, cantilever beam can be considered as pinned at the fixed end to calculate pull\_in voltage. On this basis, cantilever beam can be turned around the pinned end step by step with a fragile angle. In each step for a given voltage, total electrostatic force is compared with the restoring force so that the total electrostatic force which overrides the mechanical restoring force shows up. The restoring force is obtained by the release spring constant which is studied in Section 3.1.4.

This method is described with a flow chart (Figure 3.14) that shows how to obtain pull\_in voltage using principles of deflection obtainment. Pull\_in voltage is found 43 V using the first method which includes the load at the end principle. The second method, which uses the load at the center of gravity of the distributed load, gives the result as 62 V.



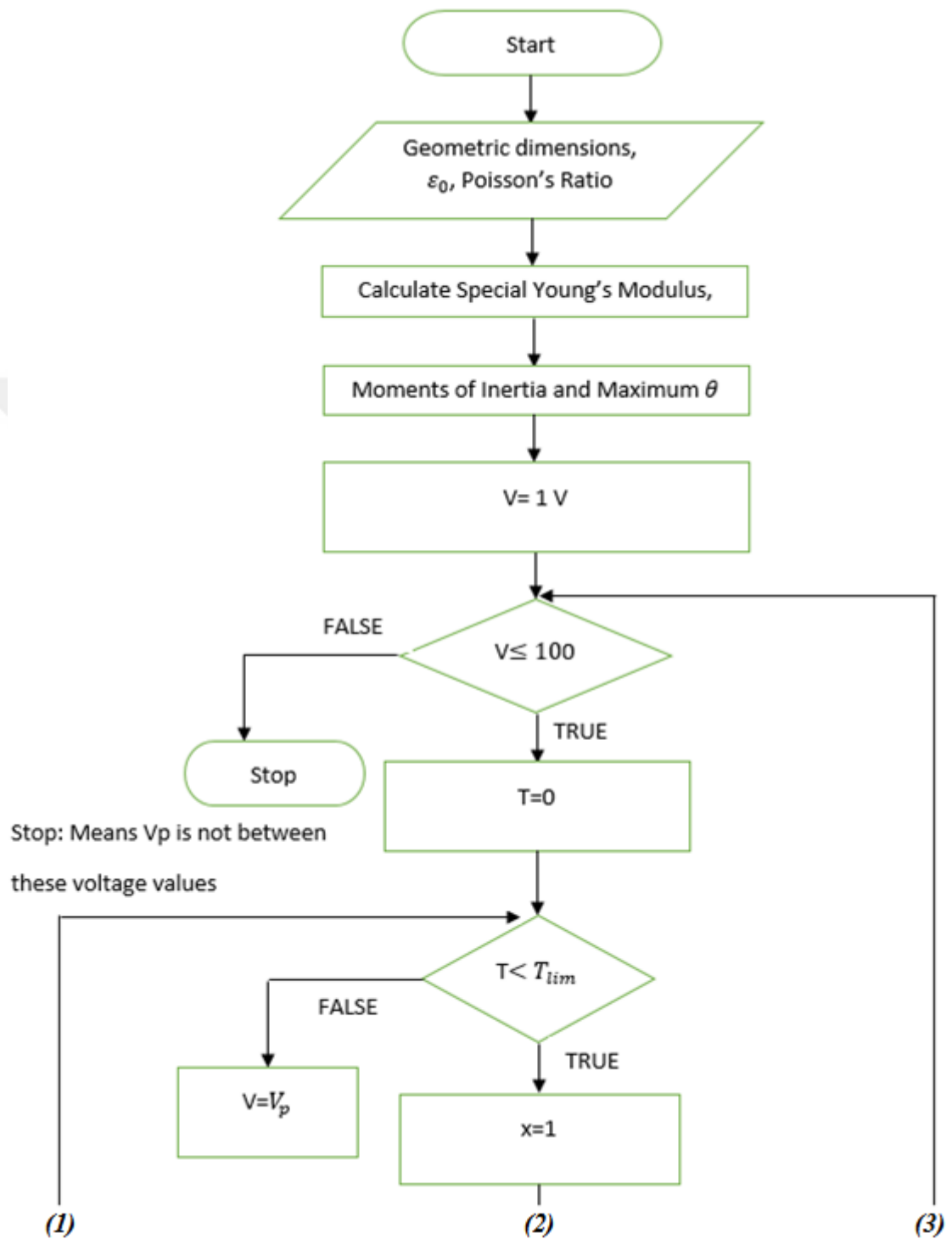


Figure 3.14 Flowchart of pull\_in voltage calculation

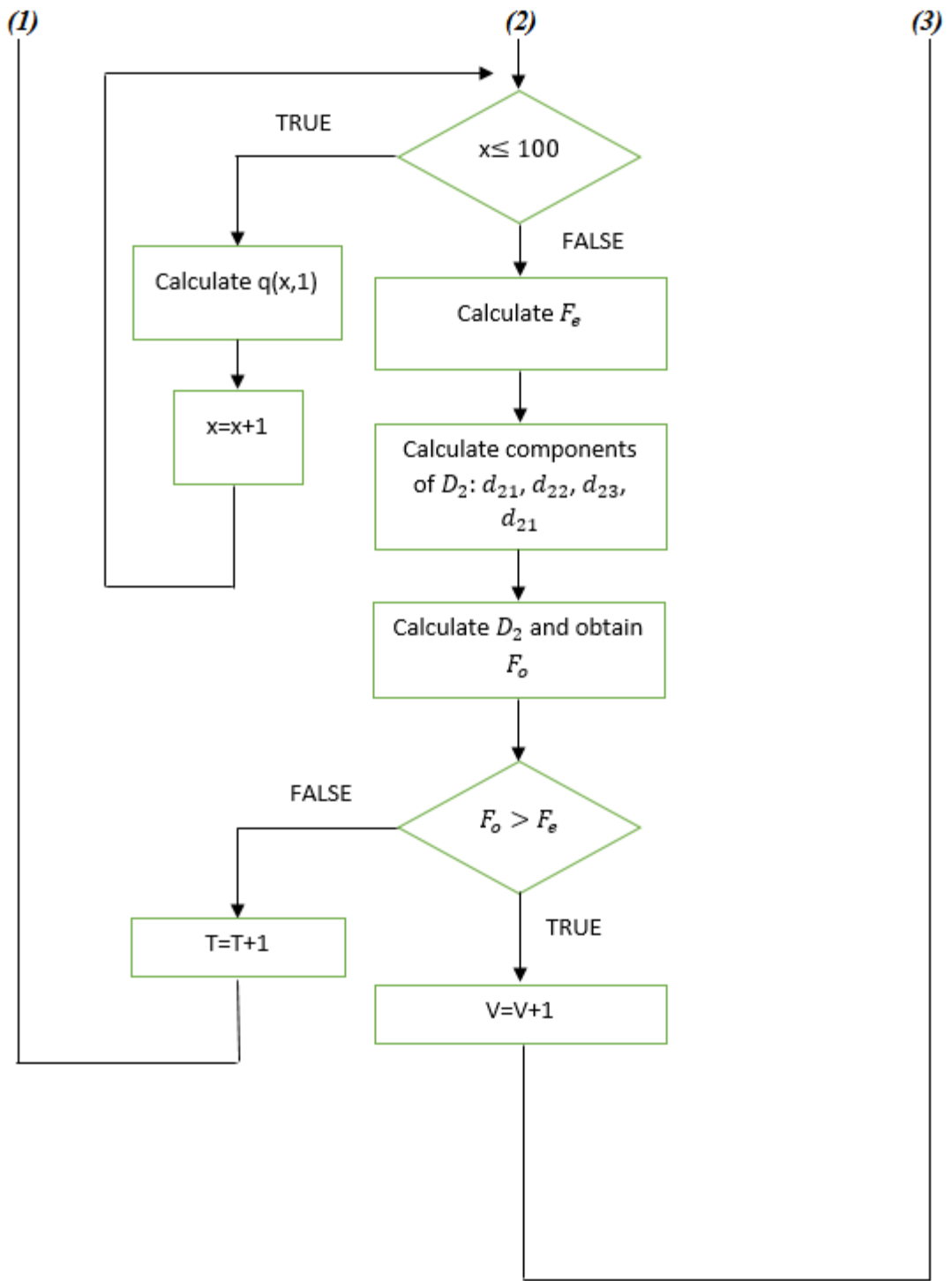


Figure 3.14 (cont.) Flowchart of pull\_in voltage calculation

Both methods can be used for estimation of pull\_in voltage. For more close result, the restoring force can be accepted in a different distance from center of gravity. MATLAB solutions show that if the concentrated load applies at  $l_0/l_2$ , pull\_in voltage is found as 52 V.

### *Hold Down Voltage*

After the beam collapses due to the applied voltage which is nearly 1.3 times bigger than the pull\_in voltage, it is not needed to apply such a big voltage anymore. Since the gap between the beam and actuation voltage becomes very little, less voltage can keep the beam in contact. This voltage value is called hold down voltage.

Hold down voltage is found with a similar fashion of pull\_in voltage calculations in MATLAB. This time, analysis starts from contact position and actuation voltage. In each steps, voltage value is decreased one by one and then total electrostatic force and release force are compared. The voltage value in which the restoring force overrides the total electrostatic force is the hold down voltage limit.

Appendix A includes the MATLAB code for hold down voltage calculation. According to this calculation, hold down voltage is found 41 V where pull\_in voltage is 43 V. Even though, the difference between them is under expectation, its reason is known. Using dimple at the free end of the beam limits the gap at contact situation. This results in closer result to pull\_in voltage for hold down voltage. It means, if no dimple is used, much lower hold down voltage can be obtained.

### **3.2.2 Contact Force**

Because the beam type is cantilever and there is no dielectric layer is used in this design, RF MEMS switch type is metal to metal contact switch and the free end of the cantilever touches the signal line metal. The amplitude of this touch is called contact force. This

touching action mostly done with a dimple which is a bulge created on the bottom face of the free end of the cantilever.

Contact force is important for the reliability. A weak contact may not be sufficient for enough safety for signal. For better contact force, more actuation voltage is needed, even so, there is a tender balance between the applied voltage and the geometry. More voltage means bigger geometry hence slower switching. As it is seen, an optimum contact force that ensures the reliability is enough.

Just like spring constant calculations, the shape of the distributed load is needed for contact force calculations, but this time, shape of the contact situation must be used.

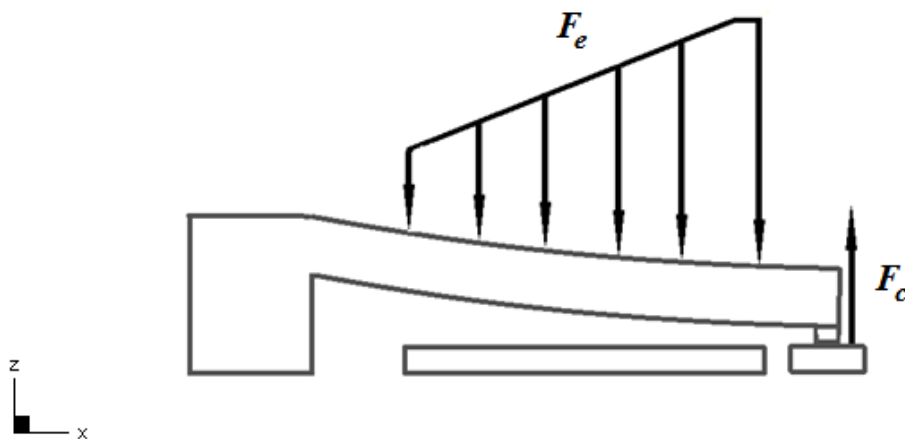


**Figure 3.15** Shape of the beam at contact situation

Obtaining the total electrostatic force  $F_e$  for contact situation – i.e. hold down position - is a little different from pull\_in situation because of the changing shape of the beam resulted from the decreasing gap between the actuation pad and the beam. For pull\_in situation, the shape of the beam was easily considered as linear. Although the form of the beam is still linear in the first contact instant, the shape of the beam starts to change after this time. New  $q$  and  $q''$  in 80 V contact situation are found just like pull\_in condition with different gap values.

The actuation voltage is 60% bigger than the pull\_in voltage, hence bigger  $F_e$  consists and leads the beam to bend more, after the free end of the cantilever contacts to contact pad (transmission line). The shape of the beam and the distributed load at contact situation are shown together in Figure 3.15.

Here, the distributed load can be considered as linear again but in a different way. The linearization may start and end from the actuation pad's alignment. In detail, a short part that is closest to the free end can be considered as parallel. The gap of the point B equals to dimple high,

$$h_{dimple} = g_B = 0.1 \mu m \quad (3.77)$$

$$g_0 = 0.3 \mu m \quad (3.78)$$

Displacement of point B,

$$d_B = g_0 - g_B = 0.2 \mu m \quad (3.79)$$

From triangle ratio,

$$\frac{d_B}{l_1 + l} = \frac{d_A}{l_1} \quad (3.80)$$

Displacement of point A,

$$d_A = 0.03 \mu m \quad (3.81)$$

Gap of point A,

$$g_A = 0.27 \text{ } \mu\text{m} \quad (3.82)$$

The actuation voltage  $V_a = 80 \text{ V}$  here is ok for a pull\_in voltage  $50 \text{ V}$ . Hence, equivalent unit loads are as follows,

$$q_1 = \frac{0.5 \times 8.85 \times 10^{-12} \times V_a^2}{g_A^2} = 3.88 \times 10^5 \text{ N/m}^2 \quad (3.83)$$

$$q_x = 18.4 \times 10^5 \text{ N/m}^2 \quad (3.84)$$

From here,

$$q_2 = 14.5 \times 10^5 \text{ N/m}^2 \quad (3.85)$$

Same linearization is also done here for  $q_x$  and total electrostatic force is found as:

$$F_e = (l - l_3)w(q_1 + 0.5q_2) = 78.9 \text{ } \mu\text{N} \quad (3.86)$$

where  $l_3$  is the length of beam part that has uniform distributed load.

In order to find the contact force, moment-area method is used [62]. Since there are four unknown variables and only three equations, the system is statically indeterminate. Moment-area method reduces the unknown variables and rest of them is solved with total moment and total force equations. The shape of the distributed load under  $80 \text{ V}$  contact situation, the reaction forces and the contact force are shown in Figure 3.16. It is mentioned before that the new beam is in fixed-simply supported type after contact.

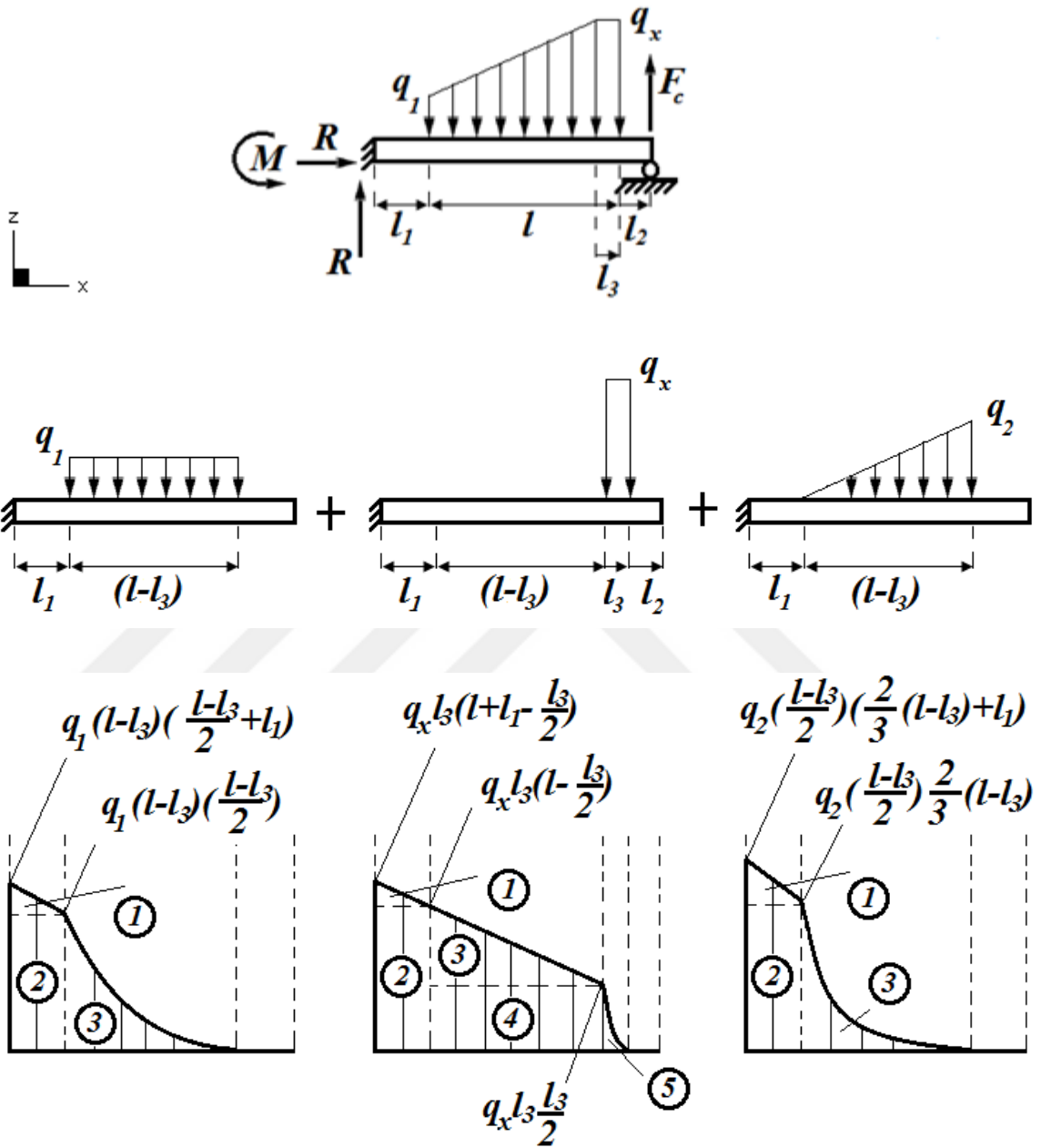
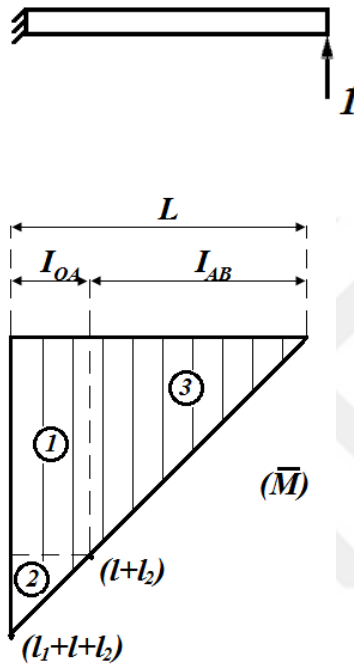


Figure 3.16 Moment diagrams of distributed load at contact situation

The distributed load is divided into three parts and moment diagrams are obtained from them. After that, a unit load that has a magnitude of 1 N is applied to the free end of the beam in opposite direction with distributed load and also its moment diagram is obtained.



**Figure 3.17** Moment diagrams of distributed load and unit load at contact situation

The reaction force at point C that equals to contact force is obtained by summation of equivalent reaction forces due to the three divided load parts,

$$F_c = C_1 + C_2 + C_3 \quad (3.87)$$

$$\delta_1 C_1 + \Delta_{1p} = 0 \quad (3.88)$$

where  $\delta_1$  equals to  $(\bar{M} \text{ area}) \times (\bar{M} \text{ center of gravity}) / EI$ ,  $\bar{M}$  is the moment area of the unit load and  $\Delta_{1p}$  equals to  $(M \text{ area}) \times (\bar{M} \text{ equivalent height}) / EI$ , where  $M$  is the



moment area of the load [62].

$$\delta_1 = \frac{(l+l_2)l_1 \frac{l_1}{2}}{EI_{OA}} + \frac{l_1 \frac{l_1}{2} \frac{2}{3} l_1}{EI_{OA}} + \frac{(l+l_2) \frac{(l+l_2)}{2} \frac{2}{3} (l+l_2)}{EI_{AB}} \quad (3.89)$$

is found for the first part that includes  $q_1$ .

$$\begin{aligned} \Delta_{1p} = & \frac{q_1(l-l_3)l_1 \frac{l_1}{2} \left( l+l_2 + \frac{2}{3}l_1 \right)}{EI_{OA}} + \frac{q_1(l-l_3) \frac{(l-l_3)}{2} l_1 \left( l+l_2 + \frac{l_1}{2} \right)}{EI_{OA}} \\ & + \frac{q_1(l-l_3) \frac{(l-l_3)}{2} \frac{(l-l_3)}{3} \left( l_2+l_3 + \frac{3}{4}(l-l_3) \right)}{EI_{AB}} \end{aligned} \quad (3.90)$$

Same solution is done for second part of the distributed load,

$$\delta_1 C_2 + \Delta_{2p} = 0 \quad (3.91)$$

$\delta_1$  is the same for all part of load.

$$\begin{aligned} \Delta_{2p} = & \frac{q_x l_3 l_1 \frac{l_1}{2} \left( l+l_2 + \frac{2}{3}l_1 \right)}{EI_{OA}} + \frac{q_x l_3 \left( l - \frac{l_3}{2} \right) l_1 \left( l+l_2 + \frac{l_1}{2} \right)}{EI_{OA}} \\ & + \frac{q_x l_3 (l-l_3) \frac{(l-l_3)}{2} \left( l_2+l_3 + \frac{2}{3}(l-l_3) \right)}{EI_{AB}} + \frac{q_x l_3 \frac{l_3}{2} (l-l_3) \left( l_2+l_3 + \frac{(l-l_3)}{2} \right)}{EI_{AB}} \\ & + \frac{q_x l_3 \frac{l_3}{2} \frac{l_3}{3} \left( l_2 + \frac{3}{4}l_3 \right)}{EI_{AB}} \end{aligned} \quad (3.92)$$

Same way for part three,

$$\delta_1 C_3 + \Delta_{3p} = 0 \quad (3.93)$$

$$\Delta_{3p} = \frac{q_2 \frac{(l-l_3)}{2} l_1 \frac{l_1}{2} \left( l+l_2 + \frac{2}{3} l_1 \right)}{EI_{OA}} + \frac{q_2 \frac{(l-l_3)}{2} \frac{2}{3} (l-l_3) l_1 \left( l+l_2 + \frac{l_1}{2} \right)}{EI_{OA}} \quad (3.94)$$

$$+ \frac{q_2 \frac{(l-l_3)}{2} \frac{2}{3} (l-l_3) \frac{(l-l_3)}{4} \left( l_2+l_3 + \frac{4}{5} (l-l_3) \right)}{EI_{AB}}$$

$$F_c = 34.67 \mu N \quad (3.95)$$

There is a closed form equation for contact force calculation and it can be used to compare the results.

$$F_c = \left( \frac{\Sigma q}{k_{act}} - \Delta g \right) x k_{rel} \quad (3.96)$$

where  $\Sigma q$  is the total distributed load under 80 V at contact situation and  $\Delta g$  is the total distance that beam passes. Substituting the variables into Eq.3.96 and

$$F_c = 25.8 \mu N \quad (3.97)$$

These two results are compared in Section 3.3

Daniel Hyman says that a contact force of a cantilevered gold metal to metal contact beam type switch must be between 50-200  $\mu N$ . Even so, this result is good enough for such a small design of beam. It is important to reduce the contact resistance for a better signal transmission, hence, for low contact resistance, to increase the contact force or contact

area is needed [63]. Figure 3.18 shows a closer drawing that describes the contact surfaces better.

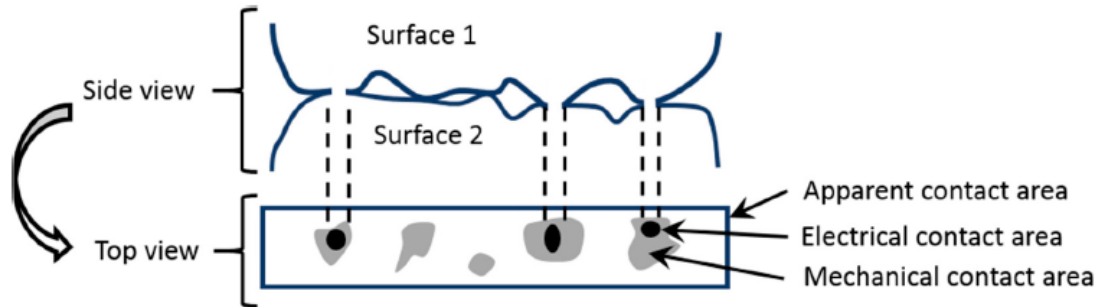


**Figure 3.18** Mechanical and electrical contact surfaces [64]

### *Reaction Force at the Fixed End of the Beam*

After finding the contact force at the free end of the beam, reaction force of fixed end can be found by total force in z direction equation.

$$+\uparrow \Sigma F_z = 0$$

$$-\Sigma q + F_c + R_z = 0 \quad (3.98)$$

Reaction force at fixed end in z direction is,

$$R_z = 44.2 \mu N \quad (3.99)$$

### **3.2.3 Release Force**

Release force, in other words restoring force, is the force that tries to get the beam to the equilibrium position at the beginning. Rebeiz acclaims the restoring force as the concentrated load that occurs at the free end of the cantilever. It is acceptable until the

contact position because during the motion beam's shape remains linear till the contact happens.

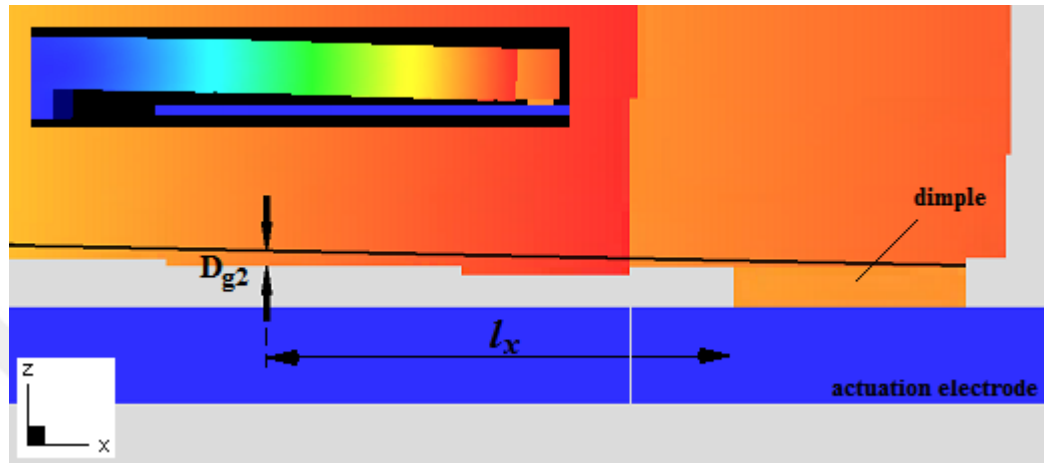


Figure 3.19 Simulation image for contact situation

However, a realistic approach must be done after contact because the shape is no more linear because the beam keeps going to bend after the contact. After contact position, there are two possible approaches to get release force. First way is to consider two forces, one of them occurs during the motion till the contact time, second one occurs after the contact time. Figure 3.20 shows these two forces whose summation is final restoring force.

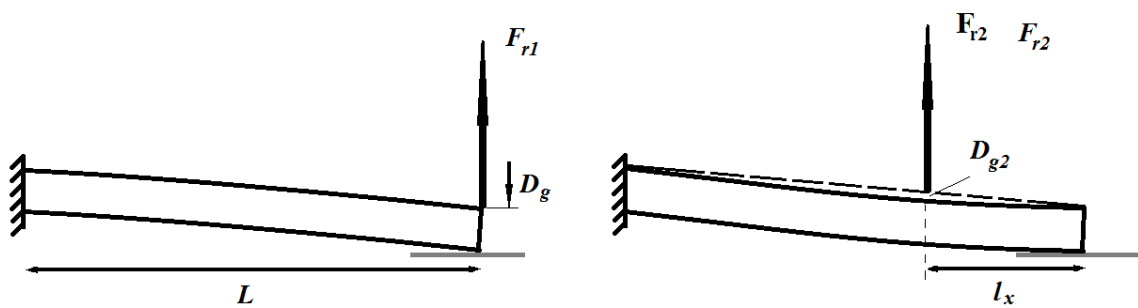


Figure 3.20 Realistic release force

$$k_{rel} = 81.9 \frac{N}{m} \quad (3.71)$$

For the first part of the total release force, Eq. 3.71 is used. The displacement is obtained by the space between dimple and ground.

$$\Delta_g = g_0 - h_{dim} \quad (3.100)$$

Clearance is found,

$$\Delta_g = 0.2 \mu m \quad (3.101)$$

It is used in release force equation,

$$F_{rel} = k_{rel} \times \Delta_g \quad (3.102)$$

Hence,

$$F_{rel} = 16.4 \mu N \quad (3.103)$$

First part of the release force is found. After contact happens, beam is no more cantilever type. It becomes fixed-simply supported beam type. Eq. 3.104 gives the displacement equation of this type of beam [59].

$$\delta_{max} = \frac{Pa}{3EI} \frac{(l^2 - a^2)^3}{(3l^2 - a^2)^2} \quad (3.104)$$

Spring constant is extracted from this equation and it must be multiplied with 0.75 because this is given for basic beams which have no hole on it.

$$k_{rel2} = \frac{3EI(3L'^2 - l_3^2)^2}{l_3(L'^2 - l_3^2)^3} \times 0.75 \quad (3.105)$$

$$\Delta_{g2} = 0.026 \mu m \quad (3.106)$$

$\Delta_{g2}$  is taken from simulation snap shot in contact situation. New length must be taken into consideration because dimple acts as anchor after the contact.

$$L' = 9.5 \mu m \quad (3.107)$$

$l_x$  is also taken from simulation,

$$l_x = 1.8 \mu m \quad (3.108)$$

Finally, second part of the restoring force can be found as,

$$F_{rel2} = k_{rel2} \times \Delta_{g2} \quad (3.109)$$

$$F_{rel2} = 57.7 \mu N \quad (3.110)$$

This is the release force due to the additional deflection that occurs after contact.

$$F_r = F_{rel} + F_{rel2} \quad (3.111)$$

Total release force is found as,

$$F_r = 74.1 \mu N \quad (3.112)$$

There is another way to obtain the restoring force. The distributed load due to the actuation voltage, which is greater than the pull\_in voltage, is known at the contact situation. If this load is applied to the beam without changing and the actuation pad under the beam is removed fictionally, beam must bend more than gap zero that is represented as  $D_{g3}$  in the Figure 3.21. So, this approach is based on dividing the distributed load into the new displacement.

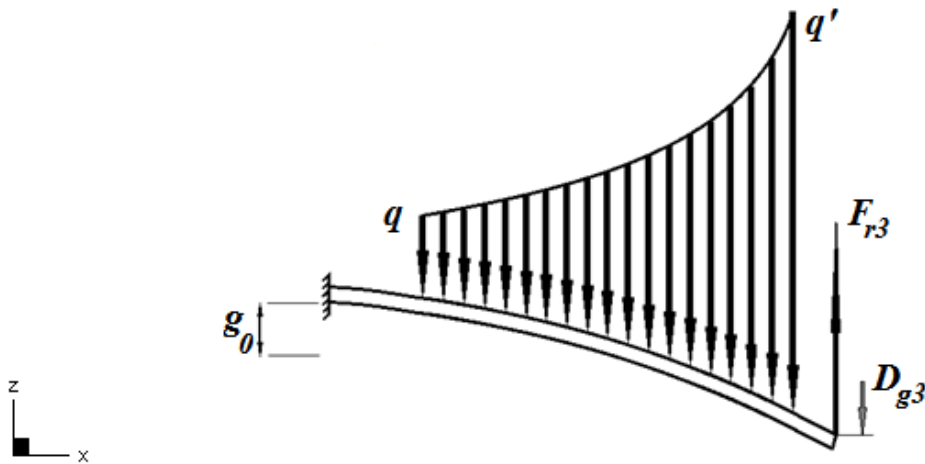


**Figure 3.21** Second restoring force approach

If there are no contact electrode, in other words if beam would be free to bend endlessly, beam would deflect as  $\Delta_{g3}$ . This new deflection can be find in a same fashion with deflection calculation (see Section 3.1.1) but this time a different distributed load is applied.

$$\Delta_{g3} = 0.47 \mu m \quad (3.113)$$

After the deflection, imaginary release force at the end of the beam can be found as follow,

$$F_{r3} = k_{rel} x \Delta_{g3} \quad (3.114)$$

Hereby, restoring force that is coming from second approach is found,

$$F_{r3} = 38.8 \mu N \quad (3.115)$$

This total release forces are used and compared with each other in release time calculation.

### 3.2.4 Resonant Frequency and Switch Time

Physically, when an external force compels a rigid body to oscillate with greater amplitude at a specific frequency, it is called resonance and frequencies at which the response amplitude is a relative maximum are known as the system's resonant frequencies [65]. Generally, the first six modes of the frequencies show the common deflection types of the body. Since the first mode represents the pure bending, it is calculated in this section.

The actuation spring constant was found in Section 3.1 and it will be used in resonant frequency calculations because the resonant frequency will be used in switching time calculation. Since the switching is about actuation, natural spring constant should not be used here.

The mass of the cantilever beam is found by:

$$m = V_{cantilever} x \rho_{gold} \quad (3.116)$$

In general mass equation is given below but a detailed calculation according to the real dimensions is done in Eq. 3.118

$$m = Lwt \rho \quad (3.117)$$

Since gold is used as material of the beam,  $\rho_{gold} = 19.32 \text{ g/cm}^3$  [66],



$$m = (10x10x1 - 4x2x1 - 2x3x1x1) \mu m^3 \times 1.932 \times 10^{-14} \frac{kg}{\mu m^3} \quad (3.118)$$

From Eq. 3.118, actual mass of the cantilever beam is,

$$m = 1.66 \times 10^{-12} \text{ kg} \quad (3.119)$$

### *Effective Mass Calculation*

Since not the whole mass of a beam is moving during the motion, effective mass of the body is needed to calculate for natural mode. Effective mass depends on the geometric specialties of the beam and mostly related to underlying pad that causes the motion [67].

$$m_{eff} = \rho \int_0^L N_{(x)}^2 A_{(x)} dx \quad (3.120)$$

From triangle ratio,

$$N_{(x)} = \frac{\delta_{(x)}}{\delta_{max}} = \frac{x}{L} \quad (3.121)$$

Since the cross-section differences are taken into consideration in actual mass calculation, area is accepted constant here,

$$m_{eff} = \rho A \int_0^L \left( \frac{x}{L} \right)^2 dx \quad (3.122)$$

$L$  comes out of the parenthesis,

$$m_{eff} = \frac{\rho A}{L^2} \left| \frac{x^3}{3} \right|_0^L \quad (3.123)$$

is found and it is integrated from 0 to  $L$ ,

$$m_{eff} = \frac{\rho AL}{3} \quad (3.124)$$

Since  $\rho AL = m$  ;

$$m_{eff} = 0.333m \quad (3.125)$$

Effective mass is found as 1/3 times the actual mass. If m is substituted into Eq. 3.125,  $m_{eff}$  is found,

$$m_{eff} = 0.553 \times 10^{-12} \text{ kg} \quad (3.126)$$

Here, the question is, which spring constant must be used? There are two options; one of them is the natural spring constant that is described in previous topic and the other one is the release spring constant that is found by the concentrated load at the end. Natural frequency equation is given by [3],

$$f_0 = \sqrt{\frac{k}{m_{eff}}} \times \frac{1}{2\pi} \quad (3.127)$$

If  $k_{rel}$  is used,

$$f_0 = 1.93 \text{ MHz} \quad (3.128)$$

If  $k_{nat}$  is used in Eq. 3.127, resonant frequency is found as follows,

$$f_{02} = 2.77 \text{ MHz} \quad (3.129)$$

For better transmission of a signal, delay must be at minimum level and the delay is mostly related to the switching time. In a good working signal system, the switching time must

be under one-tenth of a second. G. M. Rebeiz and Barker produced a formula that gives well-directed estimation for switching time without considering damping factor [3]:

$$t_s = 3.67 \frac{V_{pull\_in}}{V_{act} f_0} \quad (3.130)$$

As can be seen from the formula, the switching speed is mostly related to the actuation voltage. Generally, 1.3-1.4 times the pull\_in voltage is used for actuation for a fast switching [3]. Nevertheless, this switching time formula is given for basic beams that have a uniform geometry. In this design, there is a hole which affects the stiffness of the beam, therefore this switching time formula must be multiplied with the ratio of the stiffness for general situation. Thus, slower switch time can be obtained for a design that has higher stiffness, likewise, faster switch time can be found for a lower stiffness realistically.

$$t_s = 3.67 \frac{V_{pull\_in}}{V_{act} f_0} x \frac{k}{k_{basic}} \quad (3.131)$$

where  $k_{basic}$  is the spring constant of the designed beam without a hole and equals to 108.5 N/m. When  $f_0$  that is found by  $k_{rel}$  is used to obtain switching time,

$$t_s = 0.89 \mu s \quad (3.132)$$

### 3.2.5 Air Damping and Release Time

Another important parameter of switching is release time. It is the amount of the time that passes during the motion between the ending of the actuation voltage and settling down at equilibrium position.

$$b = \frac{3\mu(wL)^2}{2\pi g_0^3} \quad (3.133)$$

where,  $\mu$  is the coefficient of viscosity for air and is given as [3],

$$\mu = 1.845 \times 10^{-5} \quad (3.134)$$

Equation of motion is used to calculate the release time. Damping coefficient equation is given by [3],

$$F_{rel} = m_e \frac{d^2 y}{dt^2} + b \frac{dy}{dt} + k_{rel} y \quad (3.135)$$

Release force that is obtained in Section 3.2.3 can be used in equation of motion (Eq. 3.135)

$$F_{rel} = 38.8 \mu N \quad (3.136)$$

$$m_e \lambda^2 + b \lambda + k_{rel} = 0 \quad (3.137)$$

Roots of the equation are investigated,

$$\Delta = b^2 - 4m_e k_{rel} \quad (3.138)$$

$$\Delta \cong -1.706 \times 10^{-10} \quad (3.139)$$

Because of  $\Delta < 0$ , roots must be as the form of

$$\lambda_{1,2} = \alpha + i\beta \quad (3.140)$$

and roots are found as follows,

$$\lambda_{1,2} = \frac{-b \mp \sqrt{\Delta}}{2m_e} \quad (3.141)$$

First root is,

$$\lambda_1 = -2.95 \times 10^6 + 1.18 \times 10^7 i \quad (3.142)$$

Second root is,

$$\lambda_2 = -2.95 \times 10^6 - 1.18 \times 10^7 i \quad (3.143)$$

Total deflection is sum of homogeneous part and forced part of the equation of motion,

$$y = y_H + y_P \quad (3.144)$$

Homogeneous part,

$$y_H = e^{\alpha t} (c_1 e^{i\beta t} + c_2 e^{-i\beta t}) \quad (3.145)$$

Substituting the variables into Eq. 3.145

$$y_H = e^{-2.95 \times 10^6 t} (c_1 e^{1.18 \times 10^7 i t} + c_2 e^{-1.18 \times 10^7 i t}) \quad (3.146)$$

is obtained and the forced part,

$$y_P = \frac{F_{rel}}{m_e D^2 + bD + k_{rel}} \quad (3.147)$$

Since  $D = 0$ ,

$$y_p = \frac{F_{rel}}{k_{rel}} \quad (3.148)$$

Initial conditions are as follows,

$$y(0) = 0.2 \times 10^{-6} \quad (3.149)$$

$$y'(0) = 0 \quad (3.150)$$

and the constants are found as,

$$c_1 = 0.1 - 0.025i \quad (3.151)$$

$$c_2 = 0.1 + 0.025i \quad (3.152)$$

$$y = 4.89 \times 10^{-7} - \frac{1}{(2.72)^{3 \times 10^6 t}} \left[ \frac{1}{(2.72)^{12 \times 10^6 t i}} (1.44 \times 10^{-7} + 3.6 \times 10^{-8} i) \right. \\ \left. + (2.72)^{12 \times 10^6 t i} (1.44 \times 10^{-7} - 3.6 \times 10^{-8} i) \right] \quad (3.153)$$

By substituting the variables into Eq. 3.153, switch time is found,

$$t = 0.42 \text{ } \mu s \quad (3.154)$$

### 3.2.6 Stress Effect

A residual stress that is remaining from fabrication processes may occur in switch construction. If its magnitude is over limits, switch does not work properly. But if it is under acceptable limits, its effects must be calculated for reliable usage.

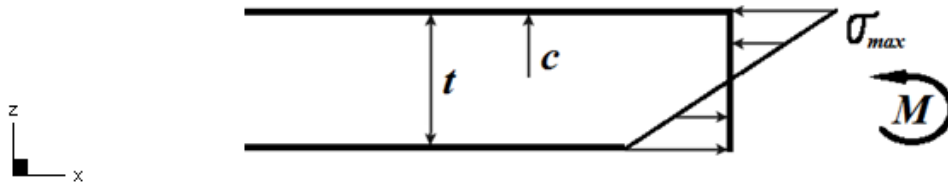


**Figure 3.22** Stress gradient at the end of the beam

The bending moment at the end of the beam that occurs due to the stress gradient is found by [7],

$$\sigma_{\max} = \frac{Mc}{I} \quad (3.155)$$

$$M = \frac{\sigma_{\max} I}{c} \quad (3.156)$$

Deflection due to the bending moment,

$$d_s = \frac{Ml^2}{2EI} \quad (3.157)$$

Substituting the variables into Eq. 3.157

$$d_s = \frac{\sigma_{\max} l^2}{2Ec} \quad (3.158)$$

In literature,  $\sigma_{\max}$ 's limit value is shown as  $5MPa$ . If it is taken into consideration,

$$d_s = 0.0115 \mu m \quad (3.159)$$

is found. This is pretty small effect for this stress gradient. If its force effect is calculated,

$$F_s = k_{rel} x d_s = 0.94 \mu N \quad (3.160)$$

is found. As it is seen, it can be ignored from deflection calculations easily, but for bigger stress gradients, this is how to obtain its effect.

### 3.3 Simulation Results of Designed Switch

Coventorware is a well-known and commonly used finite elements simulation program for designing and analyzing RF MEMS structures. It discretizes the volume of the structure into the finite elements that are joined by shared nodes. These finite elements and nodes constitute the mesh. More finite elements mean denser mesh and denser mesh means more accurate analysis. For cantilever beam design, Manhattan bricks type of mesh is preferred with an element size of 0.25-0.5  $\mu m$ . It should not be forgotten that the simulation which is done with more detailed mesh causes much longer simulation time. When the analysis is being performed, program calculates the desired values for each nodes and repeats it simultaneously using matrices.

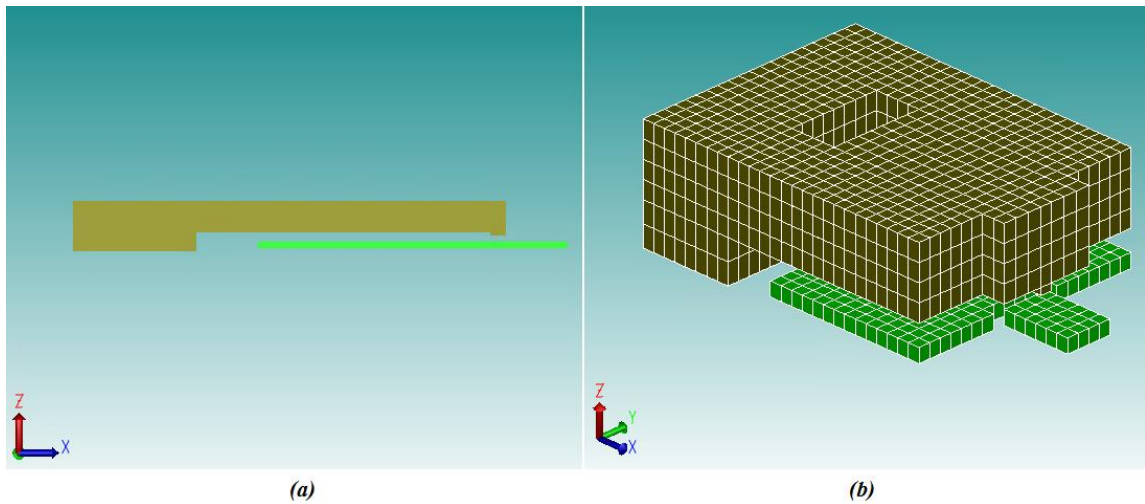


**Figure 3.23** (a) Side view of cantilever beam design (b) Meshed and 3 times extended view

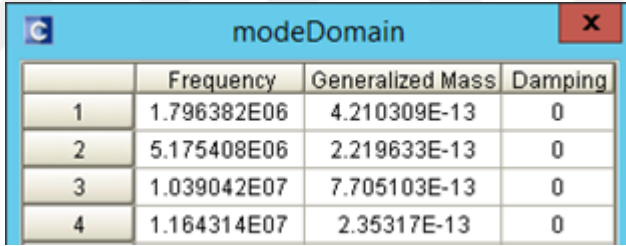


The meshed and 3 times extended in vertical axis view of the designed beam that has a rectangle hole is shown in Figure 3.23 with the side view. Beam model has a thickness of  $1 \mu m$  and sits on a  $10 \times 10 \mu m^2$  sized acreage.

The main purpose of designing is minimizing the dimensions for less actuation voltage and faster switching while keeping consider the fabrication limits. As seen from the Figure 3.23, cantilever beam model is anchored from the left end and designed for lower spring constant with hole in the width.

### *Resonant Frequency*

First analysis in Coventor is modal analysis. It gives the first six mode shapes with frequencies and effective masses. First mode that corresponds to the motion type of cantilever beam is  $1.8 MHz$ . To use this simulation, no load is required (see Figure 3.24).



	Frequency	Generalized Mass	Damping
1	1.796382E06	4.210309E-13	0
2	5.175408E06	2.219633E-13	0
3	1.039042E07	7.705103E-13	0
4	1.164314E07	2.35317E-13	0

**Figure 3.24** Resonant frequencies of the beam

### *Max. Displacement and Pull\_in Voltage*

Coventor finds pull\_in voltage by applying voltage value from  $V_{min}$  to  $V_{max}$  which are defined by user according to estimations. Figure 3.25 shows the applied voltage iterations that are increasing 10 by 10 from 0 to 60 V. Then program narrows the sensibility when it gets closer to collapse situation. In the summary table, diverge means collapse and the last displacement before the collapse instant is given in the fourth column. Pull\_in voltage is read from between last converge and first diverge value.

	ActuationElectrode_trajectory (V)	Iterations	Status	Max Displacement
Step_1	0	3	Converged	0
Step_2	10	3	Converged	2.89078E-03
Step_3	20	3	Converged	1.19854E-02
Step_4	30	3	Converged	2.88632E-02
Step_5	40	4	Converged	5.81951E-02
Step_6	50	9	Converged	1.30683E-01
Step_7	5.03125E01	5	Converged	1.38516E-01
Step_8	5.0625E01	16	Diverged	1.58813E-01
Step_9	5.125E01	7	Diverged	1.70895E-01
Step_10	5.25E01	4	Diverged	1.86875E-01
Step_11	55	4	Diverged	3.51367E-01
Step_12	60	4	Diverged	7.49055E-01

**Figure 3.25** Summary of pull\_in simulation

	ActuationElectrode_trajectory (V)	Iterations	Status	Contact	Max Displacement
Step_1	49	8	Converged	No	1.15463E-01
Step_2	4.95E01	4	Converged	No	1.22208E-01
Step_3	50	5	Converged	No	1.31019E-01
Step_4	5.05E01	8	Converged	No	1.45626E-01
Step_5	5.05625E01	4	Converged	No	1.49974E-01
Step_6	5.0625E01	10	Diverged	No	1.58239E-01
Step_7	5.075E01	7	Diverged	No	1.5986E-01
Step_8	51	5	Diverged	No	1.63631E-01

**Figure 3.26** Summary of sensitive pull\_in simulation

For closer results to the real value, sensitive pull\_in analyze must be performed with smaller voltage gaps. Sensitive pull\_in analysis indicates the pull\_in voltage which is between 50.56 V and 50.62 V, besides, maximum tip deflection is 0.149  $\mu\text{m}$  (Figure 3.26).

Beam behavior under electrostatic force is mentioned in Section 2. Beam bends under an applied voltage until the collapse instant which occurs at  $2/3 g_0$  for parallel plates. For cantilever beam, it is measured  $1/2 g_0$ . At this point, beam collapses to the ground and the

amount of the voltage indicates the shape of the beam as is seen from Figure 3.27. More voltage means more bending.

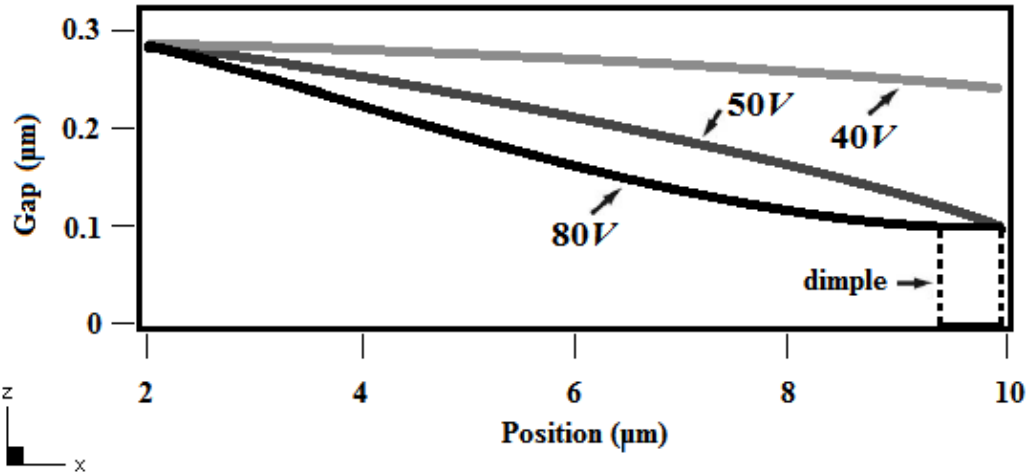


Figure 3.27 Position of figure against gap

*Electrostatic Force*

It is possible to learn from simulation that how much total distributed load occurs on the beam due to the applied voltage. It gives load results for each steps in pull\_in analysis. For pull\_in situation, total electrostatic load is found  $15.9 \mu N$ , see Figure 3.28. It can be understood from this simulation that the load that occurs in x and y directions can be ignored.

Force On Parts				
	ActuationElectrode_trajectory (V)	mechanical_F_x (uN)	mechanical_F_y (uN)	mechanical_F_z (uN)
Step_1	49	-8.03791E-02	7.653342E-05	-1.273997E01
Step_2	4.95E01	-9.318453E-02	8.146941E-05	-1.339127E01
Step_3	50	-1.110169E-01	8.758805E-05	-1.421844E01
Step_4	5.05E01	-1.432941E-01	9.874914E-05	-1.554689E01
Step_5	5.05625E01	-1.534602E-01	1.022946E-04	-1.592488E01

Figure 3.28 Total electrostatic force on the beam at collapse instant

Coventor does not give the spring constant result directly. Total electrostatic force may be divided into displacement to obtain a spring constant value from simulation.

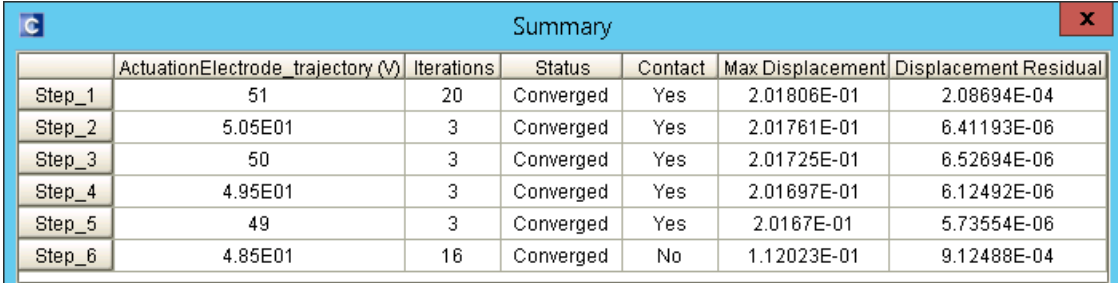
$$k_{sim} = \frac{\Sigma q}{\delta_{max}} = \frac{15.9}{0.149} \quad (3.161)$$

Spring constant that coming from simulation is found as follows,

$$k_{sim} = 106.9 \frac{N}{m} \quad (3.162)$$

### *Hold Down Voltage*

Hold-down voltage simulation is similar to pull\_in voltage simulation and it is determined as 48.5 V that can be seen from Figure 3.29. Pull\_in voltage is known from previous part. The ratio of the difference between Vhold-down and Vpull-in is similar with the solution result from Section 3.2.1. It is showed in Table 3.2 with other comparisons.



	ActuationElectrode_trajectory (V)	Iterations	Status	Contact	Max Displacement	Displacement Residual
Step_1	51	20	Converged	Yes	2.01806E-01	2.08694E-04
Step_2	5.05E01	3	Converged	Yes	2.01761E-01	6.41193E-06
Step_3	50	3	Converged	Yes	2.01725E-01	6.52694E-06
Step_4	4.95E01	3	Converged	Yes	2.01697E-01	6.12492E-06
Step_5	49	3	Converged	Yes	2.0167E-01	5.73554E-06
Step_6	4.85E01	16	Converged	No	1.12023E-01	9.12488E-04

**Figure 3.29** Summary of sensitive hold-down voltage simulation

### *Contact Force*

It is mentioned that the contact force is important for reliable signal transmission. That is why 1.6 times the pull\_in voltage is used for actuation. Figure 3.30 shows that the contact force is determined 35.55  $\mu N$ . It can be seen from simulation that, when the applied

voltage decreases, contact force decreases too. It would be zero after hold-down voltage of course.

	ActuationElectrode_trajectory (V)	Dimple_Contact_Area	Dimple_Contact_Force
Step_1	80	2.5E-01	3.555367E01
Step_2	70	2.5E-01	1.805E01

**Figure 3.30** Contact force simulation

	ActuationElectrode_trajectory (V)	Fix_Fx	Fix_Fy	Fix_Fz
Step_1	80	1.245298E00	-8.870017E-04	4.661531E01
Step_2	70	6.260994E-01	-4.713606E-04	3.362837E01

**Figure 3.31** Reaction forces of fixed end of the beam

Reaction forces at the fixed end can also be obtained from same simulation. Again, only the vertical axis can be taken into consideration. The reaction force in vertical direction is determined  $46.6 \mu N$  as is seen in Figure 3.31.

### *Switching and Release Time*

Coventor needs a time depended voltage analysis to obtain the switching time. In solver settings of the simulation program, damping coefficient is needed that belongs to the material which covers the gap like air. Program offers a damping coefficient for air and it is used in time analysis.

Actuation voltage is applied to the beam for a while and cut suddenly. Switching time is measured from zero to settling position. Release time is represented the period that passes

between the time voltage is cut and the time that beam gets to the initial equilibrium position. Although the beam keeps going to oscillate, it never touches the ground again.

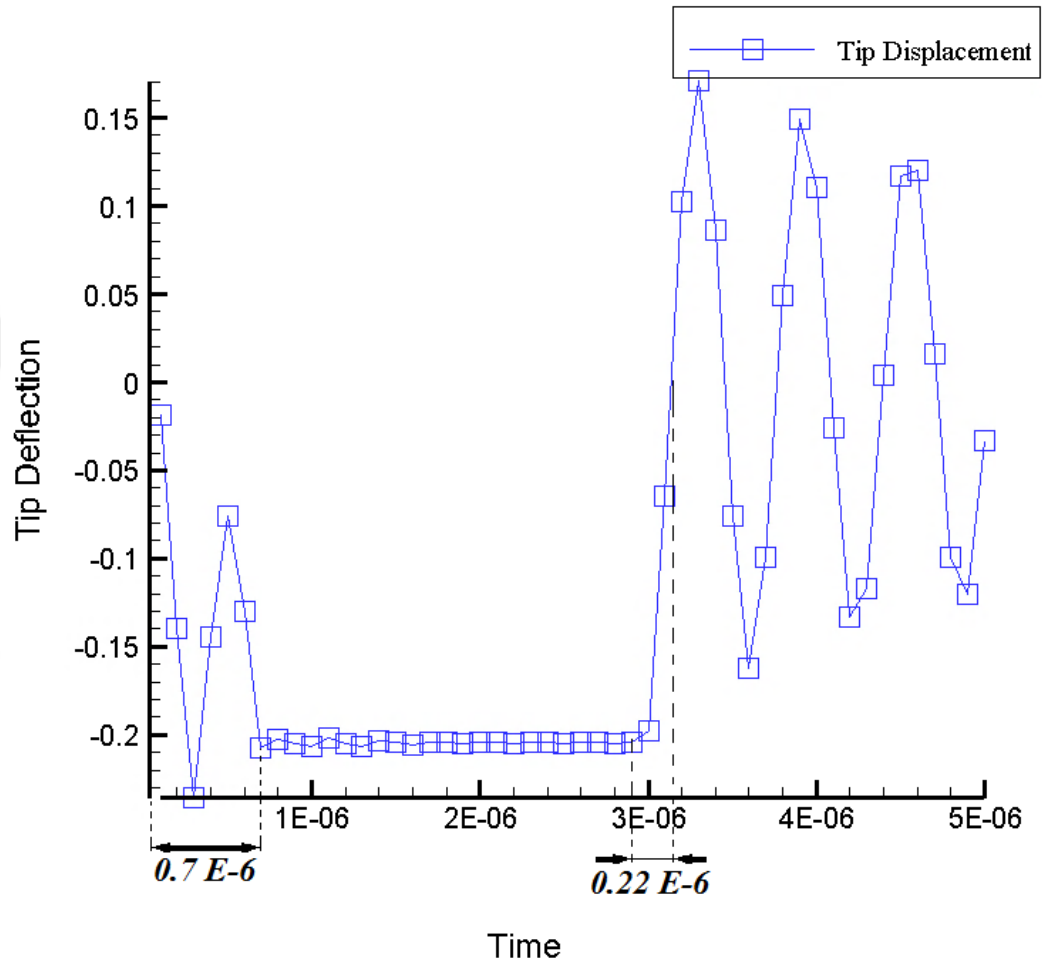


**Figure 3.32** Time analysis in Coventor

Hence, if successive voltages wanted to be applied, this release time can be taken into consideration.

Figure 3.32 shows the simulation result of time depended analysis. Switching time and release time are measured  $0.7 \mu s$  and  $0.22 \mu s$  respectively.

Table 3.2 summarizes the comparison of the parameters between simulation and analytic solutions.

**Table 3.2** Comparison of switch characteristics results for beam model

	<b>Simulation</b>	<b>Calculation</b>
Resonant frequency	1.84 MHz	1.94 MHz
Electrostatic force (50 V)	15.9 $\mu N$	17.1 $\mu N$
Electrostatic force (80 V)	81.4 $\mu N$	78.9 $\mu N$
Max. deflection	0.149 $\mu m$	0.112 $\mu m$
Pull_in voltage	50.56 V	43 V
$V_{\text{hold-down}} / V_{\text{pull-in}}$	0.96	0.95
Contact force	35.55 $\mu N$	34.7 $\mu N$
Reaction force	46.6 $\mu N$	44.2 $\mu N$
Switch time	0.7 $\mu s$	0.89 $\mu s$
Release time	0.22 $\mu s$	0.42 $\mu s$

To prove the ratio of the tip deflection to gap zero remains at  $\frac{1}{2}$ , some geometric parameters of the beam may be changed one by one and the effects of them can be measured respectively. Changing parameters are written in bold.

**Table 3.3** Simulation for different geometric parameters

	<i>t</i>	<i>g<sub>0</sub></i>	<i>w</i>	<i>l<sub>1</sub></i>	<i>l</i>	<i>l<sub>2</sub></i>	<i>a</i>	<i>V<sub>pull_in</sub></i>	<i>d<sub>max</sub></i>
<b>fundamental design</b>	1	0.3	10	2	7	1	3	50.4	0.149
<b>Model 1 sim 1</b>	1	0.3	10	2	7	1	-	65.7	0.15
<b>Model 1 sim 2</b>	1	0.3	10	2	<b>12</b>	1	3	22.21	0.135
<b>Model 1 sim 3</b>	1	0.3	<b>14</b>	2	7	1	5	55.7	0.153
<b>Model 1 sim 4</b>	1	0.3	10	<b>4</b>	5	1	3	51	0.146
<b>Model 1 sim 5</b>	1	0.3	10	2	7	1	<b>2</b>	41.6	0.145
<b>Model 1 sim 6</b>	1	<b>0.5</b>	10	2	7	1	3	108.2	0.257
<b>Model 1 sim 7</b>	<b>1.2</b>	0.3	10	2	7	1	3	65.1	0.147

Simulation 1 proves the effect of the hole on pull\_in voltage, if it was not used in beam, pull\_in voltage would be greater because of higher spring constant. Simulations 2 and 3 show the effects of length and width of the beam respectively. It is possible to say that extending the beam length and shortening the beam width makes positive effect on pull\_in voltage. It is also because of spring constant and the area of voltage actuation. Simulation 4 gives an idea about increasing the hole length. Although the opinion is to increase the hole length decreases the voltage needed, still there is a stabilizer effect of the actuation voltage area. Bigger hole means smaller actuation area and smaller area means bigger actuation voltage.



In simulation 5, the width of the hole is made wider. This results in lower pull\_in voltage while there is no compensation about actuation area or general beam acreage. Finally, the last two simulations show that to increasing neither the gap nor the thickness made pull\_in voltage smaller. This may be a predictable result but it may be helpful to see the difference ratio from fundamental model for further designs because any different situations can be met in designing.

Although it seems like the lowest pull\_in voltage came from simulation 2, it is obviously out of dimensional goals, and however it can be used easily if the geometric sizes are not cared. On the other hand, simulation 5 that uses wider hole also gives the second lowest voltage, but it may be risky to have thinner arms especially when thinking long term reliability because robustness of the beam is decreasing with thin arms. Simulations 6 and 7 show the effect of the gap and the thickness of the beam on the pull\_in voltage respectively.

From this point of view, the fundamental model can easily be considered as having most successful dimensions among others when the fabrication criteria are taken into account.

# CHAPTER 4

## CONCLUSION

In this thesis study, a basic cantilever beam type switch, which is used in RF MEMS, is designed and its mechanical parameters are calculated. Stiffness calculation method that includes superposition is also experienced with a similar design from literature [68]. The deflection result of this design is found with the same failure rate in this study. Also, release spring constant is given  $32\text{ N/m}$  in this paper and it is found  $39\text{ N/m}$  with using the release stiffness solution which is studied in this thesis. It is acceptable when it is considered that limited information is shared in literature.

Most important switch parameters are pull\_in voltage, contact force and switching time. Stiffness can be shown as the base of these parameters. For stiffness, three different types are mentioned in literature generally. They are natural stiffness, actuation stiffness and release stiffness.

Natural stiffness is acclaimed by applying a uniform distributed load to the beam, however, using this natural spring constant in resonant frequency calculation gives 54 % wrong result. On the other hand, to use the stiffness that is obtained by applying a concentrated load at the end of the beam gives much more close result to the simulation (92 %).

The release force is important to get pull\_in voltage and the restoring time. It is described in the literature as the ratio of concentrated load at the end to the deflection. It is useful while obtaining the pull\_in voltage but to obtain release time it is not enough. To solve this problem two approaches are derived and compared with each other. If the comparison is done by looking at release time results, it is seen that the restoring force model that has

two restoring force parts gives better outcome. This approach is logical because the shape of the beam is changing after contact.

The pull\_in calculation in MATLAB indicates the best place to apply restoring force is 10/12 times the length. This is a place between the center of gravity of the distributed load and end of the beam.

Another inference is about using dimple at the end of the beam. Lower hold down voltage can be reached without dimple. But this time, a good contact force may not be derived from beam without dimple. Decision must be done according to the aim of the system.

It is also understood from this study that, the closed form equation of switch time is suitable for basic designs. If a complex beam is designed, its stiffness has to be taken into consideration.

There are some differences between simulation results and calculations of some parameters like deflection. Further studies may be done to decrease these differences.

For future works, new beam types can be designed using this mechanical parameters solutions. Also, size optimization may be performed for this model to find the best or optimum pull\_in voltage and contact force values.

Furthermore, a more realistic equation can be derived for electrostatic force which can be used in non-parallel situations. Also equation of motion can be solved for switch time with forced situation instead of using closed form equation.

Above all, it is needed to fabricate the designed switch in a MEMS laboratory with clean room conditions and to package and test for usage. The most realistic comparison can only be performed with this test results. For instance, a real value of stress gradient can be determined and can be used in calculations.

# REFERENCES

- [1] Atwater, H. A., & R. W. Sudbury. "*Use of Switching  $Q$  in the Design of FET Microwave Switches.*" IEEE MTT-S International Microwave Symposium Digest, 1981.
- [2] Gopinath, Anand, & J. B. Rankin. "*GaAs FET RF switches.*" IEEE Transactions on Electron Devices 32.7: 1272-1278.APA, 1985.
- [3] Rebeiz, Gabriel M. RF MEMS: Theory, design, and technology. John Wiley & Sons, 2004.
- [4] Larson, Lawrence E., et al. "*Micromachined microwave actuator (MIMAC) technology-a new tuning approach for microwave integrated circuits.*" Microwave and Millimeter-Wave Monolithic Circuits Symposium Digest, 1991.
- [5] Goldsmith, Chuck, et al. "*Micromechanical membrane switches for microwave applications.*" IEEE Mtt S International Microwave Symposium Digest. Vol. 1. Institute Of Electrical Engineers Inc (IEEE), 1995.
- [6] Rebeiz, Gabriel M., & Jeremy B. Muldavin. "*RF MEMS switches and switch circuits.*" IEEE Microwave magazine 2.4: 59-71, 2001.
- [7] Patel, Chirag D. & Gabriel M. Rebeiz. "*RF MEMS metal-contact switches with mN-contact and restoring forces and low process sensitivity.*" IEEE Transactions on Microwave Theory and Techniques 59.5: 1230-1237, 2011.
- [8] Suganthi, S., K. Murugesan & S. Raghavan. "*CPW Dependent Loss Analysis of Capacitive Shunt RF MEMS Switch.*" Applied Computational Electromagnetics Society Journal 31.4, 2016.

- [9] Sedaghat-Pisheh, Hojr & Gabriel M. Rebeiz. "*Variable spring constant, high contact force RF MEMS switch.*" Microwave Symposium Digest (MTT), 2010 IEEE MTT-S International. IEEE, 2010.
- [10] Saha, Shimul Chandra, et al. "*Modeling of spring constant and pull-down voltage of non uniform RF MEMS cantilever.*" 2006 IEEE International Behavioral Modeling and Simulation Workshop. IEEE, 2006.
- [11] Rebeiz, Gabriel M., Guan-Leng Tan & Joseph S. Hayden. "*RF MEMS phase shifters: design and applications.*" IEEE microwave magazine 3.2: 72-81, 2002.
- [12] Wang, Z., et al. "*Contact physics modeling and optimization design of RF-MEMS cantilever switches.*" 2005 IEEE Antennas and Propagation Society International Symposium. Vol. 1. IEEE, 2005.
- [13] Saba, Norshahida, Norhayati Soin & Khairun Nisa Khamil. "*Simulation and analysis of actuation voltage of electrostatically actuated RF MEMS cantilever switch.*" Smart Sensors and Application (ICSSA), 2015 International Conference on. IEEE, 2015.
- [14] Gong, Yanjue, et al. "*Simulation and optimal design for RF MEMS cantilevered beam switch.*" Future Computer and Communication, 2009. FCC'09. International Conference on. IEEE, 2009.
- [15] Saha, Shimul Chandra, Tajeshwar Singh & T. Sasther. "*Design and simulation of RF MEMS cantilever and bridge switches for high switching speed and low voltage operation and their comparison.*" International Symposium on Signals, Circuits and Systems, 2005. ISSCS 2005.. Vol. 1. IEEE, 2005.
- [16] Fomani, A. A., S. Fouladi & R. R. Mansour. "*Magnetically-actuated dielectric cantilever RF MEMS switches.*" Microwave Symposium Digest (MTT), 2010 IEEE MTT-S International. IEEE, 2010.

- [17] Muley, Chaitali Anil & Syed A. Naveed. "*Modelling of cantilever based MEMS RF switch.*" Computing, Communications and Networking Technologies (ICCCNT), 2013 Fourth International Conference on. IEEE, 2013.
- [18] Liu, Lianjun. "*High Performance RF MEMS series contact switch-design and simulations.*" 2007 Proceedings 57th Electronic Components and Technology Conference. IEEE, 2007.
- [19] Ma, Rui, et al. "*A Dual-Polarity Graphene NEMS Switch ESD Protection Structure.*" IEEE Electron Device Letters 37.5: 674-676, 2016.
- [20] Sumant, Anirudha V., et al. "*MEMS/NEMS based on mono-, nano-, and ultrananocrystalline diamond films.*" Mrs Bulletin 39.06: 511-516, 2014.
- [21] Boodhoo, L., et al. "*Fabrication and characterization of suspended narrow silicon nanowire channels for low-power nano-electro-mechanical (NEM) switch applications.*" Microelectronic Engineering 145: 66-70, 2015.
- [22] Moldovan, Clara F., et al. "*Fabrication process and characterization of suspended graphene membranes for RF NEMS capacitive switches.*" Microelectronic Engineering 145: 5-8, 2015.
- [23] Han, Zhengli, et al. "*MEMS reconfigurable metamaterial for terahertz switchable filter and modulator.*" Optics express 22.18: 21326-21339, 2014.
- [24] Sumant, Anirudha V., et al. "*MEMS/NEMS based on mono-, nano-, and ultrananocrystalline diamond films.*" Mrs Bulletin 39.06: 511-516, 2014.
- [25] Sharma, Pankaj, et al. "*Electromagnetic performance of RF NEMS graphene capacitive switches.*" IEEE Transactions on Nanotechnology 13.1: 70-79, 2014.

- [26] DeNatale, Jeffrey & Robert Mihailovich. "*RF MEMS reliability.*" Transducers, Solid-State Sensors, Actuators and Microsystems, 12th International Conference on, 2003. Vol. 2. IEEE, 2003.
- [27] Goldsmith, C., et al. "*Lifetime characterization of capacitive RF MEMS switches.*" Microwave Symposium Digest, 2001 IEEE MTT-S International. Vol. 1. IEEE, 2001.
- [28] Lisec, T., Ch Huth & B. Wagner. "*Dielectric material impact on capacitive RF MEMS reliability.*" Microwave Conference, 2004. 34th European. Vol. 1. IEEE, 2004.
- [29] Stanimirovic, I. & Z. Stanimirovic. "*Packaging and reliability issues in microelectromechanical systems.*" Microelectronics Proceedings-MIEL 2014, 2014 29th International Conference on. IEEE, 2014.
- [30] Barbato, Marco, et al. "*Reliability of capacitive RF MEMS switches subjected to repetitive impact cycles at different temperatures.*" 2014 44th European Solid State Device Research Conference (ESSDERC). IEEE, 2014.
- [31] Mulloni, V., et al. "*Influence of fabrication tolerances on the reliability of RF-MEMS capacitive switches.*" AISEM Annual Conference, 2015 XVIII. IEEE, 2015.
- [32] Ko, C. H., et al. "*A 1.5–2.4 GHz tunable 4-pole filter using commercial high-reliability 5-bit RF MEMS capacitors.*" Microwave Symposium Digest (IMS), 2013 IEEE MTT-S International. IEEE, 2013.
- [33] Fruehling, Adam, Wei Yang & Dimitrios Peroulis. "*Cyclic evolution of bouncing for contacts in commercial RF MEMS switches.*" Micro Electro Mechanical Systems (MEMS), 2012 IEEE 25th International Conference on. IEEE, 2012.
- [34] Bouchaud, Jeremie & Henning Wicht. "*RF MEMS: status of the industry and roadmaps.*" 2005 IEEE Radio Frequency Integrated Circuits (RFIC) Symposium-Digest of Papers. IEEE, 2005.

- [35] Radant MEMS Inc., <http://www.radantmems.com/radantmems/index.html>, [01.07.2016].
- [36] MEMtronics Inc. <http://www.memtronics.com/default.aspx>, [01.05.2016].
- [37] [http://coolcosmos.ipac.caltech.edu/cosmic\\_classroom/classroom\\_activities/herschel\\_bio.html](http://coolcosmos.ipac.caltech.edu/cosmic_classroom/classroom_activities/herschel_bio.html), [01.07.2016].
- [38] <http://www.ces.fau.edu/nasa/module-2/radiation-sun.php>, [01.07.2016].
- [39] <http://www.ni.com/tutorial/3541/en/>, [01.07.2016].
- [40] [http://missionscience.nasa.gov/ems/01\\_intro.html](http://missionscience.nasa.gov/ems/01_intro.html), [01.06.2016].
- [41] Lucyszyn, S. "Review of radio frequency microelectromechanical systems technology." IEE Proceedings-Science, Measurement and Technology 151.2: 93-103, 2004.
- [42] [http://www.eeherald.com/section/designguide/mems\\_application\\_introduction.html](http://www.eeherald.com/section/designguide/mems_application_introduction.html), [01.07.2016].
- [43] Thomas, L. M., V. K. Lakdawala & K. H. Schoenbach. "Simulation studies of bulk GaAs switch photoconductivity using a picosecond laser pulse." Southeastcon'91, IEEE Proceedings of. IEEE, 1991.
- [44] Song, B. "CMOS RF circuits for data communications applications." IEEE Journal of Solid-State Circuits 21.2: 310-317, 1986.
- [45] Grant, P. D., M. W. Denhoff & R. R. Mansour. "A comparison between RF MEMS switches and semiconductor switches." MEMS, NANO and Smart Systems, 2004. ICMENS 2004. Proceedings. 2004 International Conference on. IEEE, 2004.



[46] <http://www.radio-electronics.com/info/data/semicond/varactor-varicap-diodes/basic-s-tutorial.php>, [01.07.2016].

[47] <http://www.allaboutcircuits.com/textbook/direct-current/chpt-15/magnetic-fields-and-inductance/>, [01.07.2016].

[48] [http://www.boulder.nist.gov/div853/MRD\\_Groups/MRD\\_Projects/BioMEMS\\_project.html](http://www.boulder.nist.gov/div853/MRD_Groups/MRD_Projects/BioMEMS_project.html), [01.07.2016].

[49] Saxena, Gaurav Dutta & V. Thamarai. "*Modeling and simulation of high performance sixth order sigma-delta MEMS accelerometer.*" Computational Intelligence and Communication Networks (CICN), 2011 International Conference on. IEEE, 2011.

[50] Patel, Chandradip, Patrick McCluskey & David Lemus. "*Performance and reliability of MEMS gyroscopes at high temperatures.*" Thermal and Thermomechanical Phenomena in Electronic Systems (ITherm), 2010 12th IEEE Intersociety Conference on. IEEE, 2010.

[51] Chitra, L. & V. Ramakrishnan. "*A novel design of capacitive MEMS pressure sensor for lubricating system.*" Emerging Trends In New & Renewable Energy Sources And Energy Management (NCET NRES EM), 2014 IEEE National Conference On. IEEE, 2014.

[52] Muralidhar, Y. C., et al. "*Design and simulation of polymer piezo-electric MEMS microphone.*" Circuits, Controls and Communications (CCUBE), 2013 International conference on. IEEE, 2013.

[53] Mille, V., et al. "*New technology for high throughput THz BioMEMS.*" Conference proceedings: Annual International Conference of the IEEE Engineering in Medicine and Biology Society. IEEE Engineering in Medicine and Biology Society. Annual Conference. Vol. 1. 2005.

[54] Milosavljevic, Zlatoljub D. "*RF mems switches.*" Mikrotalasna revija 10.1: 2-8, 2004.

[55] <http://spie.org/Publications/Journal/10.1117/1.JMM.14.1.015002>, [01.07.2016].

[56] <http://mwrf.com/active-components/rf-mems-switches-are-primed-mass-market-applications>, [01.06.2016].

[57] M. Zahn, *Electromagnetic Field Theory: A Problem Solving Approach*, John Wiley & Sons, New York, 1979.

[58] <https://global.britannica.com/science/permittivity>, [01.03.2016].

[59] Hibbeler, Russell C. *Statics and mechanics of materials*. Pearson Higher Ed, 2013.

[60] <http://www.awc.org/pdf/codes-standards/publications/design-aids/AWC-DA6-BeamFormulas-0710.pdf>, [01.07.2016].

[61] Chowdhury, Sazzadur, M. Ahmadi & W. C. Miller. "*Pull-in voltage calculations for MEMS sensors with cantilevered beams.*" The 3rd International IEEE-NEWCAS Conference, 2005.. IEEE, 2005.

[62] Kasımzade, Azer A. *Yapı Statiği*. Birsen Yayınevi, Türkiye, 2004.

[63] Hyman, Daniel & Mehran Mehregany. "*Contact physics of gold microcontacts for MEMS switches.*" IEEE Transactions on Components and Packaging technologies 22.3: 357-364, 1999.

[64] Peschot, Alexis, Chuang Qian & Tsu-Jae King Liu. "*Nanoelectromechanical switches for low-power digital computing.*" *Micromachines* 6.8: 1046-1065, 2015.

[65] <http://www.physicsclassroom.com/class/sound/Lesson-5/Resonance>, [01.01.2016].

[66] <http://www.chemicalelements.com/elements/au.html>, [01.01.2016].

[67] Wong, Wai Chi, Ishak Abdul Azid & Burhanuddin Yeop Majlis. "*Theoretical analysis of stiffness constant and effective mass for a round-folded beam in MEMS*

*accelerometer.*" *Strojniški vestnik-Journal of Mechanical Engineering* 57.6: 517-525, 2011.

[68] Stefanini, Romain, et al. "*Miniature MEMS switches for RF applications.*" *Journal of Microelectromechanical Systems* 20.6: 1324-1335, 2011.





# APPENDIX

# APPENDIX A

## MATLAB Code for Hold-down Voltage Determination

```
clear all; close all; clc; syms F2

g0=0.3e-6; %Gap zero
l=7e-6; %Actuation pad length
l1=2e-6; %Length of part OA
l2=1e-6; %Length of part BC
L=l1+l+l2; %Beam length
w=10e-6; %Beam width
t=1e-6; %Beam thickness
a=3e-6; %Anchor width
hd=0.1e-6; %Dimple high
E=35e9/(1-0.44^2); %Special Young's modulus
eps0=8.85e-12; %Permittivity constant
IOA=a*t^3/12; %Moment of inertia of part OA
IAB=w*t^3/24; %Moment of inertia of part AB
dmax=g0-hd; %Maximum deflection

%Calculation of deflection due to concentrated load at the end
PP=F2/2;
MM=F2*(l+l2)/2;
TT1=(PP*l1^2)/(2*E*IOA);
TT2=(MM*l1)/(E*IOA);
dd1=(PP*l1^3)/(3*E*IOA);
dd2=(MM*l1^2)/(2*E*IOA);
dd3=(TT1+TT2)*(l+l2);
dd4=(F2*(l+l2)^3)/(6*E*IAB);
DD=dd1+dd2+dd3+dd4; %Deflection

Fres=solve(DD==dmax); %Release force due to this deflection
Fr=vpa(Fres)

%Beam is divided into 100 elements in order to determine the load
for V=100:-1:0
    for x=1:1:100
        d(x)=(x/10)*1e-6*dmax/L;
        g(x)=g0-d(x); % [m]
        q(x,1)=(0.5*eps0*w*(L/100)*V^2)/g(x)^2; % [N]
    end
    for y=1:68
        C(y,1)=q(y+20,1);
    end
    Fe=sum(C);
    if Fr>Fe
        Vhold=V
        break
    end
end
end
```

# RESUME

Mahmut Cihat YILMAZ was born in Konya, in 1987. He received the BSc degree in Mechanical Engineering from Yıldız Technical University in 2011. He is currently working as a research assistant in the Department of Mechanical Engineering in Yıldırım Beyazıt University. He is still a graduate student in the Division of Mechanical Engineering of Graduate School of Natural Sciences of Yıldırım Beyazıt University.

